[(dmpe)$_2$MnH(C$_2$H$_4$)] as a Source of a Low-Coordinate Ethyl Manganese(I) Species: Reactions with Primary Silanes, H$_2$, and Isonitriles

Jeffrey S. Price, David J. H. Emslie,* Ignacio Vargas-Baca, and James F. Britten

Department of Chemistry, McMaster University, 1280 Main St. West, Hamilton, ON, L8S 4M1, Canada

Supporting Information Placeholder

ABSTRACT: Wilkinson's manganese(I) ethylene hydride complex *trans*-[(dmpe)$_2$MnH(C$_2$H$_4$)] (**1**) reacts as a source of a low-coordinate manganese(I) ethyl complex. This is illustrated in the reactivity of **1** towards a variety of reagents. Reactions of **1** with primary silanes RSiH$_3$ (R = Ph, ^{n}Bu) at 60 °C afforded ethane and the disilyl hydride manganese complexes [(dmpe)$_2$MnH(SiH$_2$R)$_2$] (**4a**: R = Ph, **4b**: R = ^{n}Bu). Additionally, reaction with H$_2$ at 60 °C afforded ethane and the dihydrogen hydride complex [(dmpe)$_2$MnH(H$_2$)] (**5**), which has previously been prepared by an alternate route. The proposed low-coordinate intermediate, [(dmpe)$_2$MnEt], was not observed spectroscopically, but could be trapped using isonitrile ligands; reaction of **1** with CNR (R = ^{t}Bu, *o*-xylyl) afforded the manganese(I) ethyl complexes [(dmpe)$_2$MnEt(CNR)] (**6a**: R = ^{t}Bu, **6b**: R = *o*-xylyl). Ethyl complex **6a** did not react further with CN^{t}Bu at 80 °C. By contrast, complex **6b** reacted with excess *o*-xylyl isonitrile to form 1,1 insertion products, including the iminoacyl complex [(dmpe)Mn(CNXyl)$_3${C(=NXyl)CEt(=NXyl)}] (**7**, Xyl = *o*-xylyl). Complexes **4a**, **6a-b**, and **7,** as well as previously reported **1** and **5**, have been crystallographically characterized, and DFT calculations have been employed to probe the accessibility of *cis* ethylene hydride and ethyl isomers of **1**.

INTRODUCTION

We previously reported reactions of the ethylene hydride complex, *trans*-[(dmpe)$_2$MnH(C$_2$H$_4$)] (**1**),[1-2] with secondary silanes (R$_2$SiH$_2$). The reaction of **1** with Et$_2$SiH$_2$ afforded the *trans* silylene hydride complex [(dmpe)$_2$MnH(=SiEt$_2$)] (**2a**) via ethane elimination.[3] By contrast, the reaction of **1** with Ph$_2$SiH$_2$ afforded ethane and [(dmpe)$_2$MnH(=SiPh$_2$)] (**2b**), as a mixture of a *trans* isomer (minor) and a *cis* isomer (major; featuring a Mn–H–Si bridging interaction), as well as [(dmpe)$_2$MnH$_2$(SiHPh$_2$)] (**3**) and Ph$_2$EtSiH (Scheme 1).[3] Compounds **2a** and **2b** are the only isolated examples of group 7 complexes bearing an unstabilized terminal silylene ligand, and the phenyl derivative (**2b**) is the first silylene hydride complex observed to exist as distinct isomers with and without a M–H–Si interaction.

The reactions to form **2a** and **2b** are considered to proceed (Scheme 1) via isomerization of **1** to yield *cis* isomer **A** followed by 1,2-insertion to generate a coordinatively unsaturated ethyl complex (**B**), reaction with H$_2$SiR$_2$ to afford a low-coordinate manganese silyl complex (**C^{SiHR2}**; formed via σ-bond metathesis or Si–H bond oxidative addition followed by C–H bond-forming reductive elimination), and finally α-hydride elimination. In the reaction of **1** with Ph$_2$SiH$_2$, the formation of complex **3** also likely proceeds via ethyl intermediate **B**. However, in this case the reaction of **B** with Ph$_2$SiH$_2$ also generates Ph$_2$SiEtH and a low-coordinate manganese hydride complex (**D**), which oxidatively adds a second equivalent of Ph$_2$SiH$_2$ (Scheme 1).

An accessible coordination site in ethyl intermediate **B** in Scheme 1 is presumably crucial to enable reactions with H$_2$SiR$_2$ reagents, and the absence of a requirement for co-ligand dissociation serves to generate a hydrosilyl complex

Scheme 1. Reactions of **1** with R$_2$SiH$_2$ (R = Et or Ph) to afford silylene hydride compounds **2a-b** and dihydrido silyl complex **3**. Species **A-D** are hypothesized intermediates.

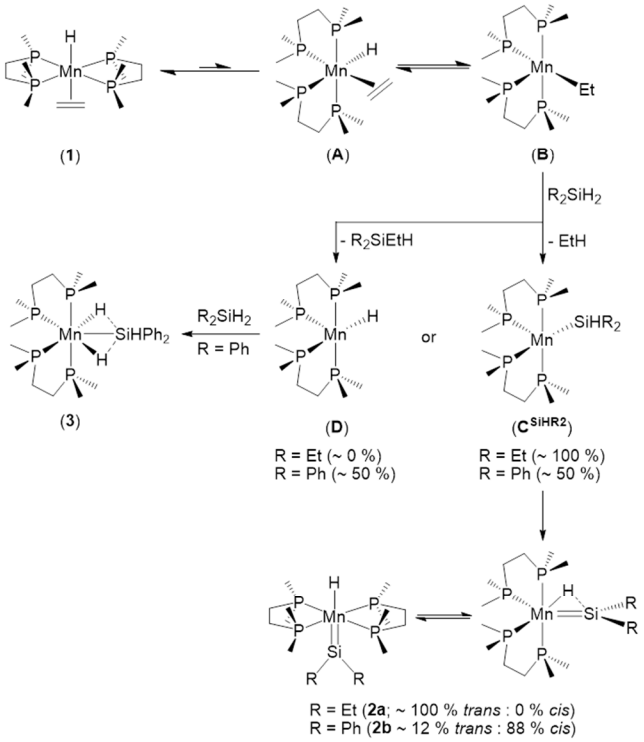

with a vacant coordination site adjacent to the silyl ligand, thereby encouraging α-hydride elimination. In fact, parallels

can be drawn between the above method for low-coordinate hydrosilyl complex generation and methods involving (a) reaction of an η^3-benzyl or η^3-allyl complex with a hydrosilane, or (b) anionic ligand abstraction from a metal hydrosilyl complex, both of which are established routes to transition metal silylene hydride complexes, proceeding via α-hydride elimination as the final reaction step.[4]

The reaction pathway in Scheme 1 relies upon conversion of alkene hydride complex **1** to a coordinatively unsaturated alkyl isomer, and such reactivity has previously been observed for a range of 2nd and 3rd row transition metal complexes. For example, the NMR spectra of isolable ethylene hydride complexes typically indicate exchange between the protons of the alkene and the hydride ligands, and in some cases (e.g. in complexes of Nb,[5-6] Ta,[6-7] W,[8] Re,[9] Os,[10] Ru,[10] Rh,[11] Ir,[12] Pd[13] and Pt[14]), reaction with a neutral donor has been shown to trap the alkyl isomer. However, in several cases, there is experimental evidence to suggest that exchange between the hydride and alkene protons occurs via a β-agostic alkyl complex, with "in-place" exchange of the bridging hydrogen atom rather than via a true low-coordinate (i.e. non-agostic) species.[14-18] This is indicated by dynamic NMR studies, including pairwise coalescence of the four ^{31}P NMR resonances observed for $[(cis\text{-}Ph_2PCH{=}CHPPh_2)_2MoH(C_2H_4)_2]^+$ at low temperature,[15] exchange of the hydride and C_2H_4 environments in $[\{\kappa^1,\eta^6\text{-}Cy_2P(o\text{-}C_6H_4)(o\text{-}C_6H_4NMe_2)\}RuH(C_2H_4)]^+$ without epimerization,[16] and exchange of the hydride and C_2H_4 environments in $[(\kappa^3\text{-POCOP})MH(C_2H_4)]^+$ {M = Rh or Ir; POCOP = o-$C_6H_3(OP^tBu_2)_2$} while maintaining top-bottom asymmetry.[17]

In contrast to ethylene hydride complexes of 2nd and 3rd row transition metals, 1st row transition metal examples are scarce (Figure 1),[2,19-23] and their isomerization to afford alkyl complexes has rarely been investigated. In fact, for the complexes in Figure 1, an equilibrium with an ethyl isomer has only been reported for the cobalt complex (though in this case calculations suggested very similar energies for the non-agostic and β-agostic cobalt ethyl structures)[15,22] and the iron cyclopentadienyl complex $[Cp^*FeH(C_2H_4)(PMe_3)]$.[19] However, from the reverse perspective, the 1st row transition metal (Sc,[24] Ti,[25-26] Ni,[27-29] and Co[30-31]) ethyl complexes in Figure 2 all feature a β-agostic C–H–M interaction, and the cobalt,[30] nickel α-diimine,[29] and nickel β-diketiminate[28] complexes undergo NMR-observable exchange of the ethyl group C*H*$_2$ and C*H*$_3$ protons and/or carbon atoms, presumably via an undetected ethylene hydride complex.

Herein we describe the reactions of *trans*-$[(dmpe)_2MnH(C_2H_4)]$ (**1**)[1] with primary silanes ($RSiH_3$; R = Ph or ^{n}Bu) and H_2 to afford disilyl hydride complexes $[(dmpe)_2MnH(SiH_2R)_2]$ (**4a**: R = Ph, **4b**: R = ^{n}Bu) and *trans*-$[(dmpe)_2MnH(H_2)]$ (**5**)[2] respectively, with liberation of ethane. This reactivity provides further support for the accessibility of a low-coordinate ethyl isomer of **1**, and we also report the X-ray crystal structure of **1**, trapping of the putative ethyl isomer via reactions of **1** with isonitrile ligands, and DFT calculations on the conversion of **1** to *cis* ethylene hydride and ethyl isomers.

RESULTS AND DISCUSSION

As reported by Girolami and Wilkinson et al. in 1983 (based on NMR spectroscopy), $[(dmpe)_2MnH(C_2H_4)]$ (**1**) exists in solution with *trans*-disposed hydride and ethylene ligands.[1] In the present work, X-ray quality crystals of **1** were obtained by recrystallization from a dilute solution in hexanes at –30 °C, and confirmed that a *trans* octahedral environment is maintained in the solid state (a in Figure 3), with the equatorial girdle of phosphine donors displaced towards the smaller hydride ligand. Complex **1** shows significant metallacyclopropane character, which is apparent from the elongated C–C distance of 1.420(2) Å (compared to 1.329 Å in ethylene and 1.535 Å in ethane).[32] The C–C distance is similar to those in previously characterized $[\{(Me_2PCH_2CH_2PMeCH_2)_2\text{-}MnH(C_2H_4)\}_2Li_4(OEt_2)_2]$ (Figure 1: bottom right) and $[Na(pmdeta)]_2[(\kappa^2\text{-}C_4H_8)Mn(C_2H_4)_2]$ (pmdeta = pentamethyldiethenetriamine) of 1.41(1)-1.444(4) Å.[2,33]

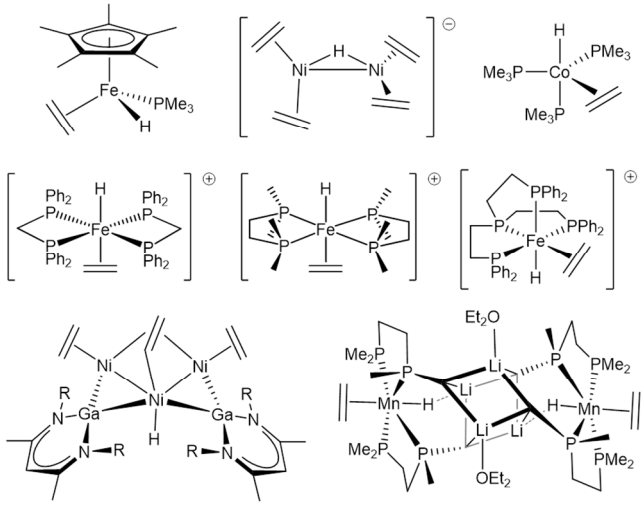

Figure 1. First row transition metal (Fe,[19-20] Ni,[21] Co[22-23] or Mn[2]) alkene hydride complexes (not including complex **1**).

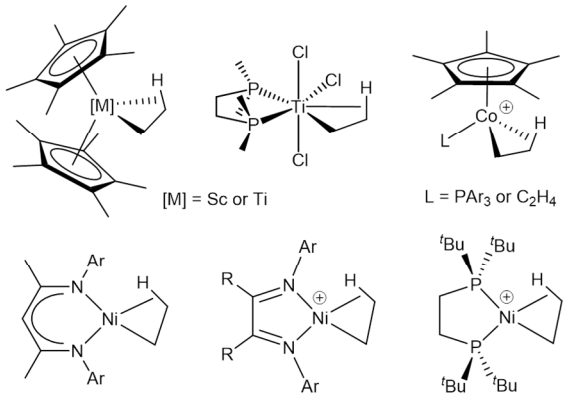

Figure 2. First row transition metal ethyl complexes reported to feature a β-agostic C–H–M interaction.[24-31]

Substantial metallacyclopropane character in **1** is also supported by DFT calculations (ADF, gas phase, all-electron, PBE, D3-BJ, TZ2P, ZORA). In particular, the C–C Mayer bond order is 1.03 (compared to 1.85 for free ethylene and 0.91 for free ethane) and in a fragment {$(dmpe)_2MnH$ and C_2H_4} interaction calculation, a substantially negative Hirschfield charge of –0.273 was observed for the ethylene fragment. Furthermore, ETS-NOCV (extended transition state method for energy decomposition analysis with natural orbitals for chemical valence) calculations on **1** partitioned the ethylene-manganese interaction into σ donation and π-backdonation contributions of 103.9 and 300.1 kJ mol^{-1} respectively.

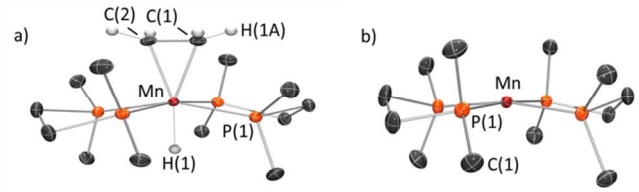

Figure 3. X-ray crystal structures of a) $[(dmpe)_2MnH(C_2H_4)]$ (**1**) and b) $[(dmpe)_2MnH(H_2)]$ (**5**) with ellipsoids drawn at 50% probability. Most hydrogen atoms have been omitted for clarity. For **1**, hydrogen atoms on the metal center and ethylene ligand were located from the difference map and refined isotropically. In the case of **5**, H and H_2 ligands were not located, and Mn is disordered over two positions, with only one conformation {51.5(1)%} shown; Mn(1A) is the Mn atom not shown in this conformation. For **1**, bond distances (Å) and angles (deg): Mn–H(1) 1.56(4), Mn–C(1) 2.123(2), Mn–C(2) 2.121(2), C(1)–C(2) 1.420(2), Σ(H–C(1)–X) (X = C, H) 349(3), Σ(H–C(2)–X) (X = C, H) 349(3), Σ(P–Mn–P) (*cis*) 356.44(4). For **5**, bond angles (deg): Σ(P–Mn(1)–P) (*cis*) 358.96(4), Σ(P–Mn(1A)–P) (*cis*) 359.13(6).

In contrast to reactions of *trans*-$[(dmpe)_2MnH(C_2H_4)]$ (**1**) with the secondary silanes Et_2SiH_2 and Ph_2SiH_2 (*vide supra*),[3] exposure of **1** to an excess of the primary silanes $PhSiH_3$ and ^{n}BuSiH$_3$ at 60°C formed the disilyl hydride complexes $[(dmpe)_2MnH(SiH_2R)_2]$ (**4a**: R = Ph, **4b**: R = ^{n}Bu) with elimination of ethane (Scheme 2).[34] Both complexes gave rise to two ^{31}P NMR resonances (60.2 and 67.4 ppm for **4a**, 58.6 and 72.6 ppm for **4b**), a single ^{29}Si NMR resonance (–4.2 and 1.6 ppm respectively), two diastereotopic Si–H ^{1}H NMR resonances (5.28 and 5.31 ppm for **4a**, 4.36 and 4.53 ppm for **4b**), and a single metal hydride ^{1}H NMR signal (–14.55 and –13.27 ppm respectively).

Scheme 2. Reactions of **1** with $RSiH_3$ (R = Ph or ^{n}Bu) or H_2 to afford disilyl hydride compounds **4a-b** and dihydrogen hydride **5**. Species **B-D** are hypothesized intermediates.

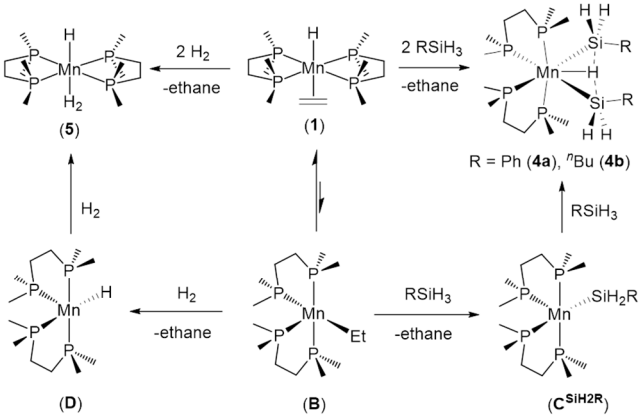

Crystals of 7-coordinate $[(dmpe)_2MnH(SiH_2Ph)_2]$ (**4a**) were obtained by cooling a saturated solution in hexanes to –30 °C, and an X-ray structure (Figure 4) revealed an octahedral arrangement of the four phosphorus and two silicon atoms about manganese, with a disphenoidal arrangement of the phosphorus donors, and the hydride ligand (located from the difference map) situated equidistant between the two silicon atoms. Complex **4a** is the first structurally characterized disilyl hydride complex of manganese with non-chelating silyl ligands, although Tobita *et. al.* previously reported a series of disilyl hydride and silyl hydrosilane complexes in which both silicon-based donors are tethered by a xanthene backbone (Figure 5).[35] The Mn–Si distance of 2.3851(2) Å in **4a** is within the range previously observed for manganese silyl hydride complexes {2.254(1)-2.4702(9) Å},[36] and is shorter than those in Tobita's most closely related disilyl hydride complex {**T3** in Figure 5: d(Mn–Si) = 2.4026(7)-2.4069(7) Å}.[35]

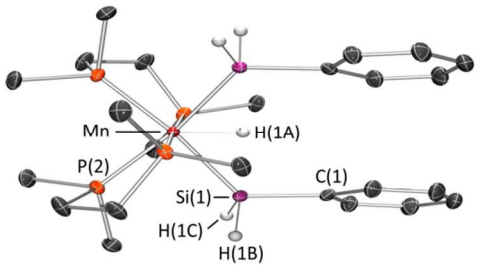

Figure 4. X-ray crystal structure of $[(dmpe)_2MnH(SiH_2Ph)_2]$ (**4a**) with ellipsoids drawn at 50% probability. Most hydrogen atoms have been omitted for clarity. Hydrogen atoms on Mn and Si were located from the difference map and refined isotropically. Dmpe ligands are disordered over two positions and only the dominant conformation {94.7(8)%} is shown. Bond distances (Å) and angles (deg): Mn–H(1A) 1.49(2), Mn–Si 2.3851(2), Si–H(1A) 1.9163(8), Si–H(1B) 1.44(2), Si–H(1C) 1.44(1), Si–Si 3.8319(4), Si–C 1.9091(7), H(1A)–Mn–Si 53.418(7), Si–Mn–Si 106.83(1).

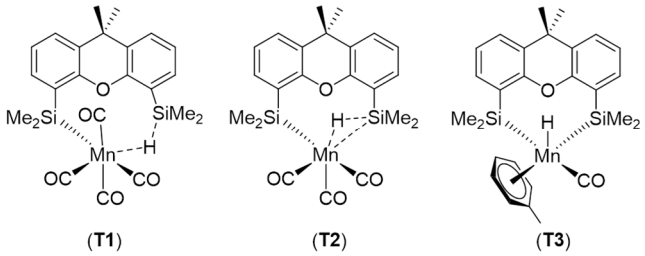

Figure 5. Disilyl hydride and silyl hydrosilane complexes reported by Tobita *et. al.*[35]

The central position of the hydride ligand between the two silyl ligands in **4a** and **4b** appears to be maintained on the NMR time scale in solution, given that the ^{1}H NMR spectra indicate C_2 symmetry between 25 and –87 °C. In the solid state (for **4a**), the Si(1)–H(1A) distance is 1.9163(8) Å (calcd: 1.92 Å), which is significantly longer than a typical Si–H single bond (1.48 Å),[37] but much shorter than the sum of the Van der Waals radii (3.1 Å).[38] The related calculated distance in a model of **4b** where ^{n}Bu groups were replaced by methyl groups (**4b***), 1.88 Å, also falls into this range. These geometries are suggestive of a nonclassical silyl hydride ligand resulting from incomplete oxidative addition to the metal center, leaving some degree of Si–H bonding intact.[39] Computationally, this bonding picture in both **4a** and **4b*** is supported by fractional Mayer bond orders for the Mn–Si (**4a**: 0.83, **4b***: 0.82-0.83), Mn–H (**4a**: 0.53, **4b***: 0.53), and Si–H_{MnH} (**4a**: 0.25-0.26, **4b***: 0.25) linkages. The magnitude of the coupling constant between ^{29}Si and the metal hydride in **4a** is 36 Hz,[40] which is consistent with either a classical or nonclassical bonding picture.[41] We were not successful in experimentally determining the sign of this coupling. However, DFT calculations afforded ^{29}Si–^{1}H coupling constants of –24 Hz (**4a**) and –27 Hz (**4b***), indicative of a nonclassical silyl

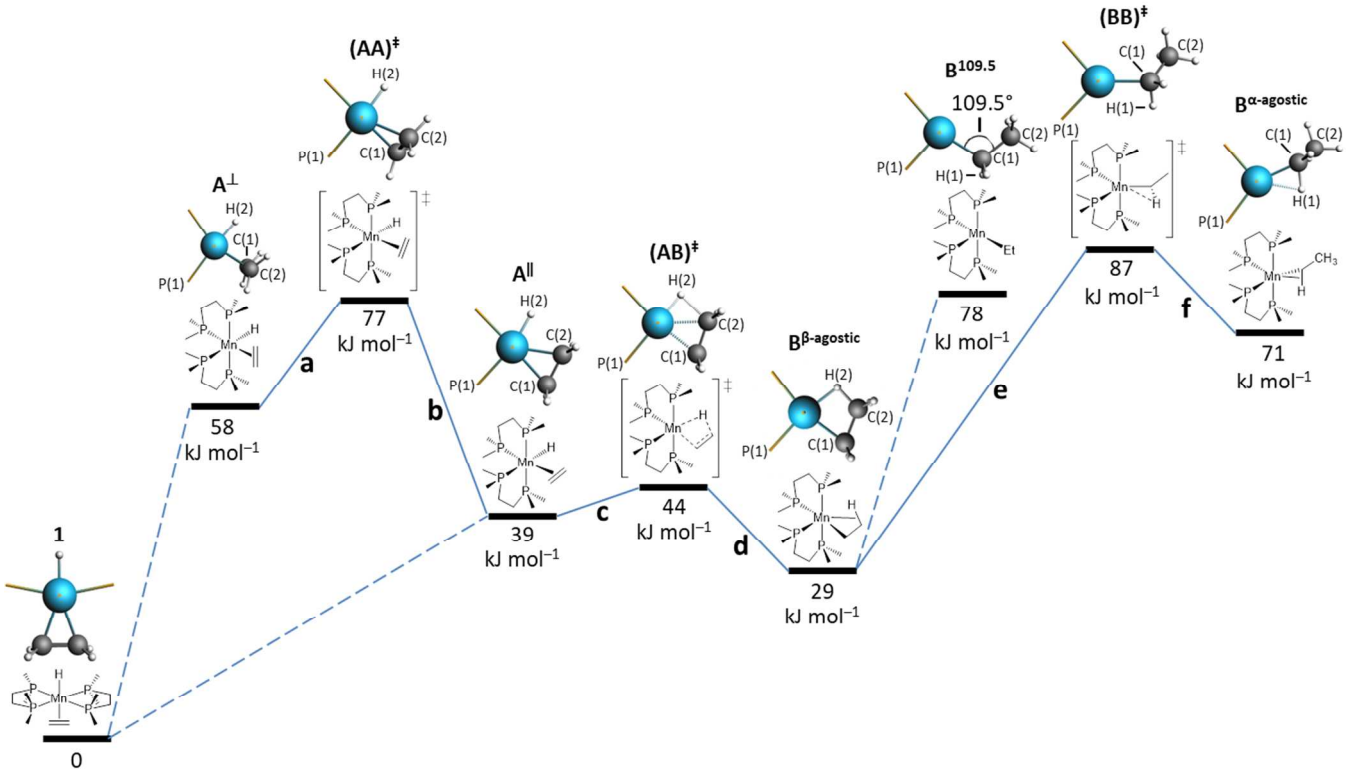

Figure 6. Potential energies (E; kJ mol^{-1}) relative to **1**, calculated for structures (left to right) i. *trans*-[(dmpe)$_2$MnH(C$_2$H$_4$)] (**1**), ii. an isomer of *cis*-[(dmpe)$_2$MnH(C$_2$H$_4$)] in which the ethylene ligand is oriented perpendicular to the plane formed by manganese, the hydride, and the ethylene centroid (**A$^{\perp}$**), iii. the transition state for isomerization of **A$^{\perp}$** to **A$^{\parallel}$** {**(AA)‡**}, iv. an isomer of *cis*-[(dmpe)$_2$MnH(C$_2$H$_4$)] in which the ethylene carbon atoms lie within the plane formed by manganese, the hydride, and the ethylene centroid (**A$^{\parallel}$**), v. the transition state for isomerization of **A$^{\parallel}$** to **B$^{\beta\text{-agostic}}$** {**(AB)‡**}, vi. [(dmpe)$_2$MnEt] with a β-agostic interaction (**B$^{\beta\text{-agostic}}$**), vii. [(dmpe)$_2$MnEt] without an agostic interaction where the Mn–C$_\alpha$–C$_\beta$ angle was restrained to 109.5° (**B$^{109.5}$**), viii. the transition state for isomerization of **B$^{\beta\text{-agostic}}$** to **B$^{\alpha\text{-agostic}}$** {**(BB)‡**}, and ix. [(dmpe)$_2$MnEt] with an α-agostic interaction (**B$^{\alpha\text{-agostic}}$**). All structures except **B$^{109.5}$** correspond to an energy minimum. The geometry optimized cores are depicted above each Chemdraw structure, showing Mn in blue, C in dark grey, and H in light grey, accompanied by stick bonds to the phosphorus donor atoms. Relative energies are those before zero-point energy (ZPE) correction.

hydride bonding environment.[41]

Compound **1** has previously been reported to be unreactive with H_2 at room temperature. However, we found that **1** does in fact react extremely slowly with H_2 at room temperature, and more rapidly at elevated temperatures (Scheme 2); [(dmpe)$_2$MnH(H$_2$)] (**5**)[2] and ethane were formed over 5 days at 60 °C in benzene, in >95% purity (77% crude isolated yield).

Complex **5** was previously prepared via the reaction of [{(dmpe)$_2$Mn(μ-AlH$_4$)}$_2$] with water,[2] and it was determined spectroscopically that the dmpe ligands are arranged equatorially with the hydride ligand *trans* to dihydrogen.[42] In this work, X-ray quality crystals of **5** (b in Figure 3) were obtained by recrystallization from a concentrated solution in hexanes at –30 °C, confirming that the dmpe ligands lie in a plane, with the manganese atom displaced 0.15-0.16 Å from the plane. Unfortunately, we were unable to locate the hydride and dihydrogen ligands in the difference map. However, DFT calculations suggest that the equatorial belt of phosphorus donors is displaced towards the hydride ligand and away from the neutral axial donor, analogous to the situation in **1**.

The syntheses of **4a-b** and **5** both produced ethane as the only byproduct, and are hypothesized to proceed via a shared low-coordinate manganese(I) ethyl intermediate, [(dmpe)$_2$MnEt] (**B**),[43] which we previously proposed as an intermediate in the syntheses of silylene hydride complexes **2a** and **2b** (Scheme 1). This intermediate would react with RSiH$_3$ or H_2 to generate a low-coordinate manganese(I) silyl (**C$^{\text{SiH2R}}$**) or hydride (**D**) complex, respectively, followed by addition of a second equivalent of RSiH$_3$ or H_2 to form **4a-b** or **5** (Scheme 2). However, neither *cis*-[(dmpe)$_2$MnH(C$_2$H$_4$)] (**A**) nor [(dmpe)$_2$MnEt] (**B**) were detected spectroscopically, so to investigate the accessibility of these complexes we turned to DFT calculations (ADF, gas phase, all-electron, PBE, D3-BJ, TZ2P, ZORA; Figure 6 and Table 1).

Geometry optimization of *cis*-[(dmpe)$_2$MnH(C$_2$H$_4$)] yielded two local minima; an isomer of lower energy, **A$^{\parallel}$**, where the ethylene carbon atoms lie within the plane formed by manganese, the hydride, and the ethylene centroid, and an isomer of higher energy, **A$^{\perp}$**, in which the ethylene ligand is perpendicular to the aforementioned plane. Isomers **A$^{\parallel}$** and **A$^{\perp}$** are interconverted by an approximate 90° rotation of the ethylene ligand {via transition state **(AA)‡**}, and are 39 and 58 kJ mol^{-1} higher in energy than the *trans* isomer (**1**) respectively (Figure 6). To probe the origin of the greater stability of **1** versus **A$^{\parallel}$** and **A$^{\perp}$**, geometry optimizations were carried out on *cis*- and *trans*-[(PH$_3$)$_4$MnH(C$_2$H$_4$)], in which steric hindrance between phosphine groups is minimized. In this case, **A$_{\text{PH3}}^{\parallel}$** (the *cis* isomer isostructural to **A$^{\parallel}$**) is lower in energy than the *trans* isomer, **1$_{\text{PH3}}$**, by 5 kJ mol^{-1}, whereas **A$_{\text{PH3}}^{\perp}$** (the *cis* isomer isostructural to **A$^{\perp}$**) is higher in energy than **1$_{\text{PH3}}$** by 22 kJ mol^{-1}. These data imply that unfavorable steric interactions between the dmpe ligands in **A$^{\parallel}$** and **A$^{\perp}$** are

Table 1. Selected angles (°), distances (Å) (and Mayer bond orders) for DFT calculated structures in Figure 6. Atom labels correspond to those in Figure 6. For alkyl isomers {$(AB)^{‡}$, $B^{\beta\text{-agostic}}$, $(BB)^{‡}$, $B^{\alpha\text{–agostic}}$, and $B^{109.5}$}; C(1) is C_α, C(2) is C_β, H(1) is the closest H on C_α to the Mn center, and H(2) is the closest H on C_β to the Mn center. For alkene hydride isomers {$A^{\perp}$, $(AA)^{‡}$, and $A^{\parallel}$}; H(2) is the metal hydride, while C(1) and C(2) are ethylene carbon atoms.

Parameter	$A^{\perp}$	$(AA)^{‡}$	$A^{\parallel}$	$(AB)^{‡}$	$B^{\beta\text{-agostic}}$	$(BB)^{‡}$	$B^{\alpha\text{-agostic}}$	$B^{109.5}$
Mn–C(1)	2.14 (0.57)	2.18 (0.53)	2.13 (0.60)	2.11 (0.66)	2.06 (0.73)	2.09 (0.75)	1.96 (0.87)	2.09 (0.83)
Mn–C(2)	2.15 (0.54)	2.16 (0.48)	2.11 (0.56)	2.12 (0.45)	2.21 (0.23)	3.17 (<0.05)	3.19 (<0.05)	2.98 (<0.05)
C(1)–C(2)	1.41 (1.05)	1.41 (1.09)	1.42 (1.06)	1.44 (1.01)	1.48 (0.95)	1.53 (0.88)	1.52 (0.89)	1.54 (0.85)
Mn–H(2)	1.58 (0.83)	1.58 (0.82)	1.56 (0.82)	1.57 (0.68)	1.71 (0.34)	3.38 (<0.05)	3.39 (<0.05)	3.14 (<0.05)
Mn–H(1)	–	–	–	2.77 (<0.05)	2.76 (<0.05)	2.50 (<0.05)	1.95 (0.20)	2.72 (<0.05)
C(2)–H(2)	2.48 (<0.05)	2.36 (0.06)	2.12 (0.13)	1.62 (0.32)	1.22 (0.68)	1.10 (0.96)	1.10 (0.96)	1.10 (0.97)
C(1)–H(1)[a]	–	–	–	1.09 (1.03)	1.09 (1.02)	1.11 (0.99)	1.16 (0.87)	1.11 (1.01)
Mn–C(1)–C(2)[b]	71.1	70.5	69.8	70.7	75.2	121.6	132.4	109.5
Mn–H(2)–C(2)	–	–	–	83.1	96.8	69.9	70.4	71.4
Mn–C(1)–H(1)	–	–	–	116.1	118.5	97.8	72.3	112.8
P(1)–Mn–C(1)	–	–	–	91.9	97.1	133.1	151.0	100.4
P(1)–Mn–C(1)–C(2)	–95.6	–133.3	174.9	173.5	171.1	136.4	98.4	171.1
Mn–C(1)–C(2)–H(2)	–41.4	–34.5	–2.8	1.0	–2.2	–54.7	–34.9	–58.4

(a) For $A^{\perp}$, $(AA)^{‡}$, and $A^{\parallel}$, all carbon–$H_{ethylene}$ distances were calculated to be 1.09 Å with Mayer bond orders ranging from 1.01 to 1.04. (b) Mn–C(2)–C(1) angles for $A^{\perp}$, $(AA)^{‡}$, and $A^{\parallel}$ are similar to the Mn–C(1)–(C2) angles: 70.3°, 71.8°, and 71.2° respectively.

responsible for their diminished stability relative to **1**. This steric penalty for adoption of a disphenoidal arrangement of the dmpe ligands also explains why **1** is isolated as a *trans* alkene hydride rather than as an ethyl isomer (despite the fact that the latter are usually lower in energy for 1st row transition metal complexes; *vide supra*), since the latter would require a disphenoidal arrangement of the dmpe ligands if an agostic interaction is to be accommodated to saturate the metal's coordination sphere (*vide infra*).

Geometry optimization of [$(dmpe)_2$MnEt] led to an energy minimum ($B^{\beta\text{-agostic}}$) featuring a β-agostic interaction to the otherwise vacant coordination site. This structure exhibits an acute Mn–C_α–C_β angle of 75.2°, a short Mn–H_β distance of 1.71 Å, an elongated C_β–H distance of 1.22 Å, and an acute (relative to a complex with an anagostic interaction) Mn–H–C_β angle of 96.8°, collectively indicative of a β-agostic interaction.[44] $B^{\beta\text{-agostic}}$ is 29 kJ mol^{-1} higher in energy than the *trans* ethylene hydride isomer (**1**), but lies 10 kJ mol^{-1} below the most stable *cis* ethylene hydride isomer ($A^{\parallel}$). Structure $B^{\beta\text{-agostic}}$ is accessed via 1,2-insertion with a transition state {$(AB)^{‡}$} only 5 kJ mol^{-1} higher in energy than starting complex $A^{\parallel}$ (Table 2). This energy barrier is quite low, but lies within the range reported for related first row transition metal complexes. For example, $\Delta E^{‡}$ was calculated to be 82 kJ mol^{-1} for [$(PMe_3)_3CoH(C_2H_4)$] and less than 2 kJ mol^{-1} for [$CpCoH(C_2H_4)(PMe_3)$]$^{+}$.[23,45]

With respect to the reactivity of an ethyl isomer of **1** with hydrosilanes or H_2, a *cis* vacant coordination site is presumably required on the metal centre, necessitating dissociation of the β-agostic interaction in $B^{\beta\text{-agostic}}$. However, no such energy minimum could be located[46]; the energy of such a species was estimated by restraining the Mn–C_α–C_β angle to 109.5°, yielding a structure ($B^{109.5}$) 49 kJ mol^{-1} higher in energy than $B^{\beta\text{-agostic}}$. This energy difference is consistent with the typical strength of a first row transition metal β-agostic interaction.[26,45] However, it differs significantly from that calculated for the ethyl isomer of [$(PMe_3)_3CoH(C_2H_4)$],[23] where the non-agostic structure was reported to be 4 kJ mol^{-1} *lower* in energy than the β-agostic isomer.

Table 2. Activation Parameters for Transformations a-f in Figure 6; $\Delta E^{‡}$ (calculated before ZPE correction), $\Delta H^{‡}$, and $\Delta G^{‡}$ (kJ mol^{-1} at 298.15 K), $\Delta ZPE^{‡}$ (kJ mol^{-1} at 0 K), and $\Delta S^{‡}$ (J mol^{-1} K^{-1} at 298.15 K)

	$\Delta E^{‡}$	$\Delta ZPE^{‡}$	$\Delta H^{‡}$	$\Delta S^{‡}$	$\Delta G^{‡}$
$A^{\perp} \rightarrow A^{\parallel}$ **(a)**	19	–0.7	17	–18	22
$A^{\parallel} \rightarrow A^{\perp}$ **(b)**	38	0.8	37	–21	44
$A^{\parallel} \rightarrow B^{\beta\text{-agostic}}$ **(c)**	5	–3.1	2	–9	4
$B^{\beta\text{-agostic}} \rightarrow A^{\parallel}$ **(d)**	15	–6.0	8	–9	11
$B^{\beta\text{-agostic}} \rightarrow B^{\alpha\text{-agostic}}$ **(e)**	58	–4.4	56	29	47
$B^{\alpha\text{-agostic}} \rightarrow B^{\beta\text{-agostic}}$ **(f)**	16	–1.9	14	12	11

A second energy minimum ($B^{\alpha\text{-agostic}}$) was located for [$(dmpe)_2$MnEt] with an obtuse Mn–$C_\alpha$–$C_\beta$ angle of 132.4°, featuring an agostic interaction between one of the α C–H bonds and the metal center. This structure features a very acute Mn–C_α–H angle of 72.3°, as well as a short Mn–H_α distance of 1.95 Å, and a slightly elongated C_α–H_α distance of 1.16 Å. Conversion of $B^{\beta\text{-agostic}}$ to $B^{\alpha\text{-agostic}}$ not only involves cleavage of the β-agostic interaction and establishment of an α-agostic interaction, but also migration of the Mn–C bond into the position previously occupied by the β-agostic interaction, with concomitant Mn–C_α–C_β angle expansion and rotation about the Mn–C_α and C_α–C_β bonds (Table 1). $B^{\alpha\text{-agostic}}$ is 42 kJ mol^{-1} higher in energy than $B^{\beta\text{-agostic}}$, and is accessed via a transition state {$(BB)^{‡}$} located 58 kJ mol^{-1} higher in energy than $B^{\beta\text{-agostic}}$ (Table 2), so could conceivably play a role in the reactivity of **1** with hydrosilanes or H_2. This energy barrier lies within the 44–85 kJ mol^{-1} range calculated for this type of isomerization in a series of Co(III) ethyl cations derived from

$\{[(C_5R'_5)CoH(C_2H_4)(PR_3)]^+$; R = Me or $P(OMe)_3$, R' = H or Me$\}$.[47]

The largest activation energy associated with conversion of **1** to $\mathbf{B}^{\beta\text{-agostic}}$ or $\mathbf{B}^{\alpha\text{-agostic}}$ is presumably associated with *trans* to *cis* isomerization of **1** (i.e. conversion of **1** to either isomer of **A**; likely via a 5-coordinate intermediate formed by phosphine or ethylene dissociation), rather than 1,2-insertion to convert $\mathbf{A}^{\mathbf{I}}$ to $\mathbf{B}^{\beta\text{-agostic}}$ or isomerization of $\mathbf{B}^{\beta\text{-agostic}}$ to $\mathbf{B}^{\alpha\text{-agostic}}$, since the activation barriers for the latter two transformations are only 5 and 58 kJ mol^{-1} respectively (Figure 6, Table 2).

In pursuit of experimental corroboration for the accessibility of [$(dmpe)_2$MnEt] (**B**) from *trans*-[$(dmpe)_2MnH(C_2H_4)$] (**1**), a trapping experiment was conducted with *tert*-butyl isonitrile (CN^tBu) at 50 °C, affording [$(dmpe)_2$MnEt(CN^tBu)] (**6a**) (Scheme 3). This reaction initially formed a low-symmetry species identified by NMR spectroscopy as the *cis* isomer of **6a**, featuring ^{1}H NMR resonances for two diastereotopic MnCH_2 protons (–0.12 and 0.22 ppm; Figure 7) and three broad ^{31}P NMR signals (61.6, 74.4, and 81 ppm; broadening is presumably due to reversible isonitrile or phosphine donor dissociation in solution). Upon cooling to 207 K, the ^{31}P signals sharpened and one signal split into two, giving the expected four ^{31}P environments. At the temperature of synthesis (50 °C), ***cis*-6a** slowly converted into ***trans*-6a** (Scheme 3), which gave rise to a single sharp ^{31}P NMR signal at 74.7 ppm and an apparent octet in the ^{1}H NMR spectrum due to the MnCH_2 protons (0.47 ppm; apparent octet due to very similar $^3J_{H,H}$ and $^3J_{H,P}$ coupling to the adjacent CH_3 group and 4 equivalent phosphines; Figure 7). This *cis*-*trans* isomerization did not proceed to completion, but an equilibrium was established (over many days at 50 °C, or a few hours at 80 °C), dominated by ***trans*-6a**. The reaction to form complex **6a** is, to the best of our knowledge, only the second example where an ethyl complex could be trapped by Lewis base addition to an isolable 1st row transition metal ethylene hydride complex.[19] Complex **6a** shows surprising thermal stability for a β-hydrogen containing alkyl complex; in solution, negligible decomposition was observed after 12 hours at 80 °C.

Scheme 3. Reactions of **1** with isonitriles to afford ethyl complexes **6a-b** and further insertion products, including **7**.

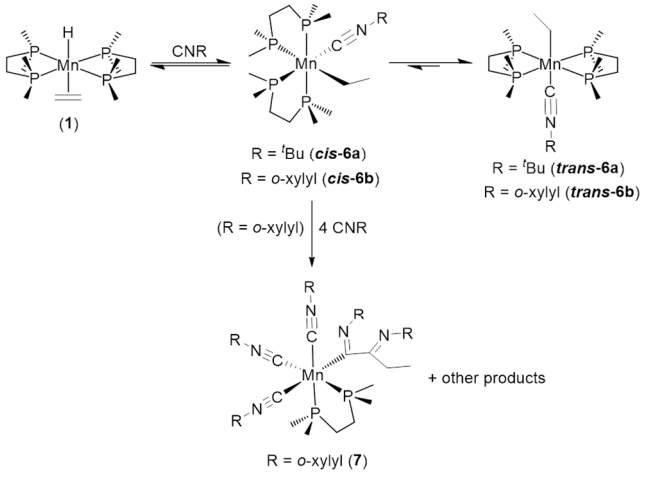

Assignment of the two species produced in the reaction of **1** with CN^tBu as isomers of **6a**, as opposed to iminoacyl complexes, was corroborated by the observation of NMR coupling between the α ethyl protons and the ^{31}P nuclei, indicating the close (in this case, 3 bond) proximity of these nuclei. Upon ^{31}P decoupling of the ^{1}H NMR spectrum, the multiplets associated with the MnCH_2 environments collapsed to signals with the expected ^{1}H-^{1}H coupling; doublets ($^2J_{H,H}$ = 11 Hz) of quartets

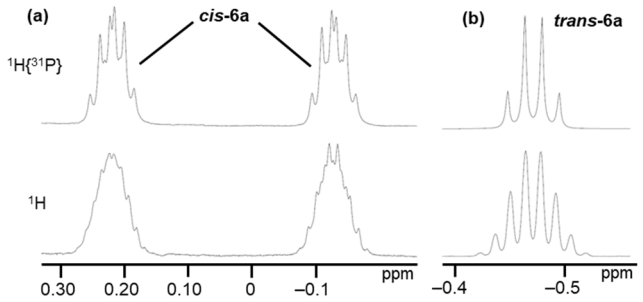

Figure 7. Regions of the ^{1}H{^{31}P} (above) and ^{1}H (below) NMR spectra for the MnCH_2 environments in a) *cis*-[$(dmpe)_2$MnEt(CN^tBu)] (***cis*-6a**) and b) *trans*-[$(dmpe)_2$MnEt(CN^tBu)] (***trans*-6a**).

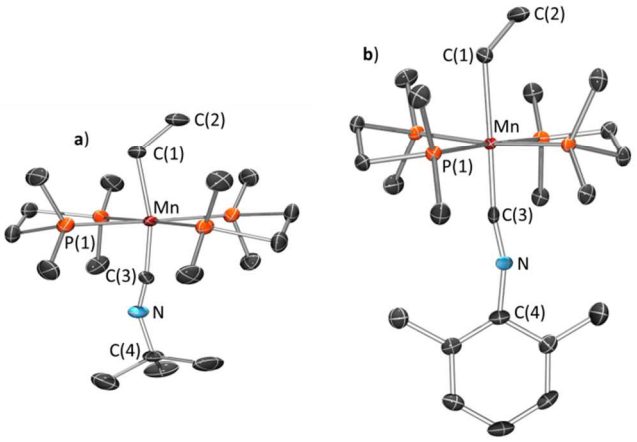

Figure 8. X-ray crystal structures of a) *trans*-[$(dmpe)_2$MnEt(CN^tBu)] (***trans*-6a**) and b) *trans*-[$(dmpe)_2$MnEt(CNXyl)] (***trans*-6b**) with ellipsoids drawn at 50% probability. Hydrogen atoms have been omitted for clarity. In the case of ***trans*-6a**, all atoms except P and Mn are disordered over two positions, and only one conformation {50.1(2)% and 52.8(2)% for the two dmpe ligands, 50.5(2)% for the isonitrile ligand, and 56.0(3)% for the ethyl ligand} is shown. In the case of ***trans*-6b**, one dmpe ligand and the N atom are both disordered over two positions, and only one conformation {51.4(3)% for the dmpe ligand and 55(2)% for N} is shown. Atoms below with an 'A' suffix are the atoms related to those with the same identifying number without a suffix, but in the conformation not shown in the figure. For ***trans*-6a**, bond distances (Å) and angles (deg): Mn–C(1) 2.222(2), Mn–C(1A) 2.226(3), Mn–C(3) 1.803(4), Mn–C(3A) 1.813(3), C(1)–C(2) 1.528(4), C(1A)–C(2A) 1.526(6), C(3)–N(1) 1.207(5),[48] C(3A)–N(1A) 1.214(4),[48] N(1)–C(4) 1.456(5), N(1A)–C(4A) 1.458(5), Mn–C(3)–N(1) 168.2(6),[48] Mn–C(3A)–N(1A) 171.0(6),[48] C(3)–N(1)–C(4) 148.3(5),[48] C(3A)–N(1A)–C(4A) 146.0(5),[48] Mn–C(1)–C(2) 120.4(2), Mn–C(1A)–C(2A) 120.6(3), Σ(P–Mn(1)–P) (*cis*) 360.04(4). For ***trans*-6b**, bond distances (Å) and angles (deg): Mn–C(1) 2.212(2), Mn–C(3) 1.794(2), C(1)–C(2) 1.520(4), C(3)–N(1) 1.223(7), C(3)–N(1A) 1.219(9), N(1)–C(4) 1.391(7), N(1A)–C(4) 1.394(9), C(1)–Mn–C(3) 174.1(1), Mn–C(3)–N(1) 173.1(7), Mn–C(3)–N(1A) 165.4(6), C(3)–N(1)–C(4) 159(1), C(3)–N(1A)–C(4) 159(1), Mn–C(1)–C(2) 122.8(2), Σ(P–Mn(1)–P) (*cis*) 360.34(6).

($^3J_{H,H}$ = 7 Hz) for the diastereotopic MnCH_2 protons of ***cis*-6a**, and a quartet ($^3J_{H,H}$ = 8 Hz) for the MnCH_2 protons of ***trans*-6a** (Figure 7).

In contrast to the clean reactivity of **1** with CN^{t}Bu, the reaction of **1** with *o*-xylyl isonitrile (CNXyl, Xyl = *o*-xylyl) produced a mixture of products (Scheme 3), including a minor product identified by X-ray crystallography and NMR spectroscopy as *trans*-[(dmpe)$_2$MnEt(CNXyl)] (***trans*-6b**; b in Figure 8). A low concentration of a short lived, low symmetry, species was also observed, and is presumed to be the *cis* isomer of [(dmpe)$_2$MnEt(CNXyl)] (***cis*-6b**), with two ^{1}H signals for the diastereotopic MnCH_2 environments at 0.03 and 0.27 ppm, and an apparent triplet for the MnCH_2CH_3 environment (1.92 ppm, $^3J_{H,H}$ = 8 Hz). DFT calculations support the thermodynamic accessibility of both *cis*- and *trans*- isomers of ethyl complexes **6a-b** in solution, given that the former are only 12-18 kJ mol^{-1} higher in energy than the latter.

Both ***trans*-6a** and ***trans*-6b** were characterized by X-ray diffraction (Figure 8), and are the first crystallographically characterized examples of terminal manganese ethyl complexes, although [Mn(μ-Et)$_4${Li(tmeda)}$_2$], which features ethyl ligands bridging between Mn and Li centers, has been reported.[49] In the solid state, these manganese(I) ethyl complexes feature an octahedral environment around the manganese center, with the ethyl ligand *trans* to the isonitrile ligand. X-ray crystal structures of ***trans*-6a** and ***trans*-6b** also feature notably acute C–N–C angles {**6a**: 146.0(5)°-148.3(5)°;[48] **6b**: 159(1)°}, long N–$C_{terminal}$ distances {**6a**: 1.207(5)-1.214(4) Å;[48] **6b**: 1.22(1) Å}, and short Mn–C_{CNR} bonds {**6a**: 1.803(4)-1.813(3) Å; **6b**: 1.793(3) Å}, consistent with strong π-backdonation from the electron rich "(dmpe)$_2$MnEt" fragment to the isonitrile ligand.[50]

Attempts to purify either of the two isomers of **6b** from the reaction mixture failed, and the additional products formed in the reaction of **6b** with CNXyl are presumed to result from phosphine substitution by excess *o*-xylyl isonitrile and/or multiple isonitrile insertion reactions. Support for these reaction pathways was provided by crystallization of [(dmpe)Mn(CNXyl)$_3${C(=NXyl)CEt(=NXyl)}] (**7**) from the reaction mixture, which features an octahedral coordination environment composed of a single dmpe ligand, three isonitrile ligands, and a κ^1-C(=NXyl)CEt(=NXyl) ligand *trans* to one of the isonitriles (Figure 9 and Scheme 3).[51] NMR spectra of complex **7**, which could be isolated in approximately 90% purity, show two ^{31}P NMR signals (53.9 and 66.2 ppm) and three xylyl-Me ^{1}H NMR signals (correlating to four ^{13}C NMR signals in the ^{1}H–^{13}C HSQC spectrum) integrating to a total of five isonitrile ligands per dmpe ligand and ethyl substituent. Unlike ethyl complexes **6a-b**, the MnCH_2 environment in the ^{1}H NMR spectrum of **7** displays no coupling to ^{31}P, due to a separation of 5 bonds between the MnCH_2 protons and phosphorus.

SUMMARY AND CONCLUSIONS

Previously, we reported reactions of *trans*-[(dmpe)$_2$MnH(C_2H_4)] (**1**) with secondary silanes to form unexpected silylene hydride products and ethane. This reactivity was proposed to take place via an undetected low-coordinate manganese ethyl species, [(dmpe)$_2$MnEt] (**B**), and in this work we provide support for this mechanism via DFT calculations and trapping experiments with isonitriles to afford [(dmpe)$_2$MnEt(CNR)] (**6a**: R = ^{t}Bu, **6b**: R = *o*-xylyl). Furthermore, compound **1** was shown to react with primary silanes or H_2 to afford the disilyl hydride complexes [(dmpe)$_2$MnH(SiH_2R)$_2$] (**4a**: R = Ph, **4b**: R = ^{n}Bu), and the dihydrogen hydride complex [(dmpe)$_2$MnH(H_2)] (**5**). These reactions also release ethane, consistent with σ-bond metathesis or oxidative addition/reductive elimination reactivity stemming from **B**.

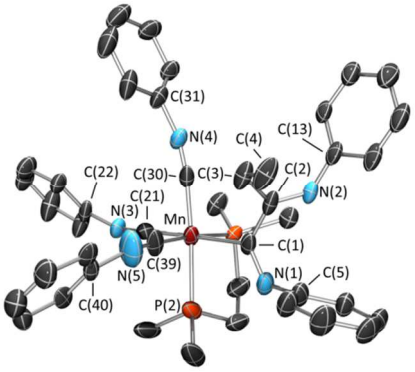

Figure 9. X-ray crystal structure of [(dmpe)Mn(CNXyl)$_3${C(=NXyl)CEt(=NXyl)}] (**7**), with ellipsoids drawn at 50% probability. Methyl groups on the *o*-xylyl ligands and all hydrogen atoms have been omitted for clarity. The phenyl group of one isonitrile ligand is disordered over two positions and only the dominant conformation {51.4(6)%} is shown. C(40A) is the counterpart to C(40) in the conformation not shown. Bond distances (Å) and angles (deg): Mn–C(1) 2.110(5), Mn–C(21) 1.837(5), Mn–C(30) 1.848(6), Mn–C(39) 1.832(6), C(1)–C(2) 1.522(8), C(2)–C(3) 1.540(7), C(3)–C(4) 1.522(7), C(1)–N(1) 1.307(6), C(2)–N(2) 1.291(6), N(1)–C(5) 1.425(7), N(2)–C(13) 1.419(7), C(21)–N(3) 1.198(7), C(30)–N(4) 1.198(6), C(39)–N(5) 1.133(6), N(3)–C(22) 1.408(6), N(4)–C(31) 1.401(6), N(5)–C(40) 1.486(5), N(5)–C(40A) 1.49(1), Mn–C(1)–C(2) 120.2(3), Mn–C(1)–N(1) 121.2(4), C(1)–N(1)–C(5) 125.3(5), C(2)–C(3)–C(4) 113.4(5), C(2)–N(2)–C(13) 123.6(4), C(1)–C(2)–C(3) 118.6(4), C(1)–C(2)–N(2) 117.8(4), Mn–C(21)–N(3) 175.8(5), Mn–C(30)–N(4) 171.9(4), Mn–C(39)–N(5) 177.3(5), C(21)–N(3)–C(22) 160.3(5), C(30)–N(4)–C(31) 166.5(5), C(39)–N(5)–C(40) 155.1(5), C(39)–N(5)–C(40A) 169.7(6).

The reactions of **1** with primary silanes differ from those with secondary silanes in that disilyl hydride complexes are formed rather than silylene hydride complexes. Compounds **4a** and **4b** are of interest in their own right as nonclassical complexes in which oxidative addition is incomplete, leaving appreciable bonding character between the hydride and silyl ligands (based on calculated ^{29}Si–^{1}H NMR coupling constants and bond orders, as well as the crystallographically determined distance between silicon and the manganese hydride in **4a**). Furthermore, isolated ethyl complex **6a** is a rare example of a thermally stable β-hydride-containing alkyl complex, showing negligible decomposition over 12 hours at 80 °C.

This work contributes to fundamental understanding of the equilibrium between transition metal ethylene hydride and ethyl complexes. As described in the introduction, 1st row transition metal ethylene hydrides are extremely scarce (the equilibrium typically lies to the side of the ethyl isomer), and the equilibrium between ethylene hydride and alkyl complexes has rarely been investigated. Compound **1** provided a unique opportunity to study this process, and key computational findings are (a) two isomers of a *cis* ethylene hydride are energeti-

cally accessible from **1** ($\mathbf{A}^{\perp}$ and $\mathbf{A}^{\parallel}$), differing in the orientation of the alkene relative to the plane formed by manganese, the hydride, and the ethylene centroid, (b) the *trans* ethylene hydride isomer (**1**) is 39 kJ mol^{-1} lower in energy than the most energetically favorable *cis* isomer ($\mathbf{A}^{\parallel}$), primarily due to increased steric hindrance between the dmpe ligands in either isomer of **A**, (c) the most energetically favorable *cis* ethylene hydride complex ($\mathbf{A}^{\parallel}$) is 10 kJ mol^{-1} higher in energy than the β-agostic ethyl isomer ($\mathbf{B}^{\beta\text{-agostic}}$), (d) the barrier to 1,2-insertion, converting $\mathbf{A}^{\parallel}$ to $\mathbf{B}^{\beta\text{-agostic}}$, is only 5 kJ mol^{-1}, (e) an α-agostic ethyl isomer ($\mathbf{B}^{\alpha\text{-agostic}}$) is energetically accessible, 42 kJ mol^{-1} higher in energy than $\mathbf{B}^{\beta\text{-agostic}}$, (f) the barrier to conversion of $\mathbf{B}^{\beta\text{-agostic}}$ to $\mathbf{B}^{\alpha\text{-agostic}}$ is 58 kJ mol^{-1}, and (g) an energy minimum for a non-agostic ethyl complex with a *cis* vacant coordination site was not located, but a structure optimized with the Mn–C_α–C_β angle restrained to 109.5° ($\mathbf{B}^{109.5}$) was 49 kJ mol^{-1} higher in energy than $\mathbf{B}^{\beta\text{-agostic}}$.

EXPERIMENTAL SECTION

General Details. An argon-filled MBraun UNIlab glove box equipped with a –30 °C freezer was employed for the manipulation and storage of all oxygen- and moisture- sensitive compounds. Air-sensitive preparative reactions were performed on a double-manifold high-vacuum line equipped with a two stage Welch 1402 belt-drive vacuum pump (ultimate pressure 1×10^{-4} torr) using standard techniques.[52] The vacuum was measured periodically using a Kurt J. Lesker 275i convection enhanced Pirani gauge. Commonly utilized specialty glassware included thick walled flasks equipped with Teflon stopcocks, and J-Young or Wilmad-LabGlass LPV NMR tubes. A VWR Clinical 200 Large Capacity Centrifuge (with 28° fixed-angle rotors that hold 12 × 15 mL or 6 × 50 mL tubes, in combination with VWR high-performance polypropylene conical centrifuge tubes) located within a glove box was used where indicated. Residual oxygen and moisture was removed from the argon stream by passage through an Oxisorb-W scrubber from Matheson Gas Products.

Benzene, diethylether, pentane, octane, and hexamethyldisiloxane were purchased from Aldrich, hexanes and toluene were purchased from Caledon, and deuterated solvents were purchased from ACP Chemicals. Benzene, diethylether, pentane, octane, hexamethyldisiloxane, hexanes and toluene were initially dried and distilled at atmospheric pressure from sodium/benzophenone (first six) or sodium (toluene). All solvents were stored over an appropriate drying agent (hexamethyldisiloxane, benzene, diethylether, toluene, d^8 toluene, C_6D_6 = Na/Ph_2CO; hexanes, pentane = Na/Ph_2CO/tetraglyme) and introduced to reactions or solvent storage flasks via vacuum transfer with condensation at –78 °C.

Dmpe, $PhSiH_3$, ^{n}BuSiH_3, 1,4-dioxane, *tert*-butyl isonitrile, *o*-xylyl isonitrile, and (trimethylsilyl)methylmagnesium chloride solution (1.0 M in diethyl ether) were purchased from Sigma-Aldrich. Manganese dichloride was purchased from Strem Chemicals. Argon and hydrogen gas were purchased from PraxAir. [$(dmpe)_2MnH(C_2H_4)$] (**1**) was prepared according to the literature.[2]

NMR spectroscopy (^{1}H, ^{1}H{^{31}P}, ^{13}C{^{1}H}, ^{29}Si{^{1}H}, ^{29}Si, ^{31}P{^{1}H}, NOESY/EXSY, TOCSY, ^{1}H–^{1}H-COSY, ^{1}H–^{13}C-HSQC, ^{1}H–^{13}C-HMBC, ^{1}H–^{29}Si-HSQC, ^{1}H–^{29}Si-HMBC, ^{1}H–^{31}P-HMBC) was performed on Bruker AV-500, AV-600, and AV-850 spectrometers. Spectra were obtained at 300 K unless otherwise indicated. All ^{1}H NMR spectra were referenced relative to $SiMe_4$ through a resonance of the proteo impurity of the solvent used: C_6D_6 (δ 7.16 ppm) and d^8 toluene (δ 2.08 ppm, 6.97 ppm, 7.01 ppm, and 7.09 ppm). Also, all ^{13}C NMR spectra were referenced relative to $SiMe_4$ through a resonance of the ^{13}C in the solvents: C_6D_6 (δ 128.06 ppm) and d^8 toluene (δ 20.43, 125.13, 127.96, 128.87, and 137.48 ppm). The ^{29}Si NMR spectra were referenced using an external standard of hexamethyldisiloxane in $CDCl_3$ (6.53 ppm), and the ^{31}P NMR spectra were referenced using an external standard of 85% H_3PO_4 in D_2O (0.0 ppm).

Unsuccessful attempts to experimentally determine the sign of the coupling constants between the metal hydride and silicon in **4b** were conducted using ^{1}H–^{1}H COSY NMR spectroscopy (850 MHz, 32 scans). This method involves locating cross-peaks between the terminal Si*H* and metal hydride NMR signals. A line could then be drawn between the two ^{29}Si satellites on one of these cross-peaks (going through the parent cross-peak); a positive slope would indicate that both coupling constants involving ^{29}Si (to the terminal Si*H* and to the metal hydride signals) have the same sign, and a negative slope would be indicative of opposite signs. A single bond coupling between ^{29}Si and a terminal Si*H* signal is known to be negative, so a positive slope would indicate a negative ^{29}Si–H_{MnH} coupling constant and a negative slope would indicate a positive ^{29}Si–H_{MnH} coupling constant.[41,53]

Combustion elemental analyses were performed by the London Metropolitan University in London, UK, and by Midwest Microlabs in Indianapolis, USA. IR spectra were performed on transmission mode on a Nicolet 6700 FT-IR spectrometer as a suspension in Nujol, and on a Bruker Tensor 27 IR spectrometer as a solution in octane, in both cases using CaF_2 plates (for solution measurements, a liquid cell purchased from International Crystal Laboratories was used).

All calculated structures were fully optimized with the ADF DFT package (SCM, versions 2014.05 to 2017.207).[54] Calculations were conducted in the gas phase within the generalized gradient approximation using the 1996 Perdew-Burke-Ernzerhof exchange and correlation functional (PBE),[55] using the scalar zeroth-order approximation (ZORA)[56] for relativistic effects, and Grimme's DFT-D3-BJ dispersion correction.[57] Input coordinates for **1**, **4a**, **5**, and ***trans*-6a-b** were derived from X-ray crystal structures. Input coordinates for **4b*** were derived by modifying the X-ray crystal structure of **4a**, input coordinates for $\mathbf{A}^{\perp}$, $\mathbf{A}^{\parallel}$, $\mathbf{B}^{\beta\text{-agostic}}$, $\mathbf{B}^{\alpha\text{-agostic}}$, and $\mathbf{B}^{109.5}$ were derived by modifying the calculated ***cis*-6a** structure, input coordinates for $\mathbf{B}^{trans}$ were derived by modifying the X-ray crystal structure of ***trans*-6b**, input coordinates for the transition state calculations were derived from linear transit calculations, input coordinates for free isonitriles were derived by modifying the X-ray crystal structures of ***trans*-6a** and ***trans*-6b**, and input coordinates for $\mathbf{1}_{PH3}$, $\mathbf{A}_{PH3}{}^{\perp}$, and $\mathbf{A}_{PH3}{}^{\parallel}$ were derived by modifying the geometry optimized structures of **1**, $\mathbf{A}^{\perp}$, and $\mathbf{A}^{\parallel}$ respectively. Preliminary geometry optimizations were conducted with frozen cores corresponding to the configuration of the preceding noble gas (core = medium) using double-ζ basis sets with one polarization function (DZP), a Voronoi grid with an integration value of 5, and default convergence criteria for energy and gradients. These structures were further refined using all-electron triple-ζ basis sets with two polarization functions (TZ2P) and fine integration grids (Voronoi 7 or Becke[58] good-quality).

Unless otherwise noted, reported values in this work correspond to restricted calculations (for modelling diamagnetic structures). For 5-coordinate structures $\mathbf{B}^{trans}$, $\mathbf{B}^{\beta\text{-agostic}}$, $\mathbf{B}^{\alpha\text{-agostic}}$, $\mathbf{B}^{109.5}$, and $\mathbf{(BB)}^{\ddagger}$, a second set of calcluations was conducted to model a potential paramagnetic structure using the UNRESTRICTED command[59] in conjunction with forcing 2 unpaired electrons (using the CHARGE command) and explicit occupation numbers (using the OCCUPATIONS command).

Bond orders were calculated within the Mayer,[60] Gopinathan-Jug,[61] and Nalewajski-Mrozek[62-63] formalisms. Visualization of the computational results was performed using the ADF-GUI (SCM) or Biovia Discovery Studio Visualizer. Bonding between the '$(dmpe)_2MnR$' (R = H, Et) moiety and neutral ethylene in **1** or isonitrile ligands in the two isomers of **6a-b** was analyzed in detail by fragment calculations (Ziegler-Rauk Energy Decomposition Analysis[64] and the ETS-NOCV method[63,65]). In such calculations, fragments had structures as calculated in each optimized whole molecule. Relaxation (optimization) of the individual fragments yielded the preparation energy, i.e. the energetic cost of geometric distortion of the interacting fragments. BSSE values were not calculated, as their contribution is negligible for large interacting molecules.

Analytical frequency calculations[66] were conducted on all geometry optimized structures (including geometry optimized fragments) to ensure that the geometry optimization led to an energy minimum and to obtain thermodynamic parameters. In a handful of cases, slightly negative frequencies (frequency range from –24 to –22 cm^{-1}, and absorption intensity range from –0.98 to –0.17 km mol^{-1}) were ob-

served but were shown to be spurious imaginary frequencies using the SCANFREQ command.[67]

Transition states were optimized by minimizing energy gradients while ensuring that the Hessian had a negative eigenvalue for the normal coordinate that contains atomic motions consistent with the transformation (using the TransitionState subkey in the Geometry key block).

NMR coupling constants were calculated (using geometry optimized coordinates derived as discussed above) with the CPL program of the ADF package[68] from wave functions obtained by hybrid PBE0[69] (ZORA)[56] calculations using the TZ2P basis sets with additional steep basis functions (TZ2P-J). This method was benchmarked against published data calculated for related nonclassical silyl hydride complexes. The literature results[41] were reproduced with acceptable accuracy for [(C_5H_4Me)MnH($SiHPh_2$)($CO)_2$] (this work: –52 Hz, literature calcd.: –68 Hz, literature expt.: –63 Hz[41]), [$Cp_2TiH(SiHPh_2)(PMe_3)$] (this work: –22 Hz, literature calcd.: –28 Hz, literature expt.: |28| Hz[70]), and [$Cp_2TiH(SiHClPh)(PMe_3)$] (this work: 19 Hz, literature calcd.: 23 Hz, literature expt.: 15 Hz[53]).

Single-crystal X-ray crystallographic analyses were performed on crystals coated in Paratone oil and mounted on either a Bruker SMART APEX II diffractometer with a 3 kW sealed-tube Mo generator and SMART6000 CCD detector (**1**, **4a**, **5**, **6a**) or on a STOE IPDS II diffractometer with an image plate detector (**6b**, **7**) in the McMaster Analytical X-Ray Diffraction Facility (MAX). A semi-empirical absorption correction was applied using redundant data. Raw data was processed using XPREP (as part of the APEX v2.2.0 software), and solved by either direct (SHELXS-97)[71] or intrinsic (SHELXT)[72] methods. The structures were completed by difference Fourier synthesis and refined with full-matrix least-squares procedures based on F^2. In all cases, non-hydrogen atoms were refined anisotropically and hydrogen atoms were generated in ideal positions and then updated with each cycle of refinement {with the exception of hydrogen atoms on Mn or Si (all complexes except **5**), or C(1) and C(2) of **1**, which were located from the difference map and refined isotropically}. Refinement was done using Olex2.[73]

Complexes **1** and **4** – **7** are air sensitive, and products observed upon reaction with air are malodorous. Therefore, all syntheses were conducted under an atmosphere of argon. Care should be taken in syntheses which generate ethane in a sealed flask (**4a-b**): the volume of the flasks used should be chosen to accommodate the ethane produced without leading to unreasonably high pressures. All isolated complexes in this work were diamagnetic.

[(dmpe)$_2$MnH($SiH_2Ph)_2$] (4a). An excess of phenylsilane (770 mg, 7.12 mmol) was added to a solution of [(dmpe)$_2$MnH(C_2H_4)] (**1**) (543.7 mg, 1.41 mmol) in 30 mL of toluene. The reaction mixture was stirred in a 100 mL sealed flask at 60 °C for 4 h, after which time the solvent was removed *in vacuo* leading to a dark orange oil. Note that ethane is formed as a by-product in this reaction, so after 30 minutes, the reaction mixture was temporarily allowed to cool to room temperature and the excess gas was vented into the Schlenk line before continuing heating at 60 °C. Washing twice with 10 mL of hexanes produced a yellow solid, which was dissolved in 9 mL of toluene and residual solid was removed by centrifugation. Layering the resulting solution with 20 mL of hexanes and storing at –30 °C for days afforded large orange crystals of **4a** with a yield of 63% (509.2 mg, 0.89 mmol). Note that on some occasions, instead of large orange crystals a yellow powder was obtained. X-ray quality crystals were obtained from a saturated solution of **4a** in hexanes at –30 °C. ^{1}H NMR (C_6D_6, 600 MHz, 300 K): δ 8.12 (d, 4H, $^3J_{H,H}$ 7 Hz, *o*), 7.31 (t, 4H, $^3J_{H,H}$ 7 Hz, *m*), 7.24 (t, 2H, $^3J_{H,H}$ 7 Hz, *p*), 5.31 (s with ^{29}Si sat., 2H, $^1J_{H,Si}$ 158 Hz, Si*H*), 5.28 (s with ^{29}Si sat., 2H, $^1J_{H,Si}$ 167 Hz, Si*H*), 1.50 (d, 6H, $^2J_{H,P}$ 5 Hz, PCH_3), 1.39 (m, 2H, PCH_2), 1.16 (m, 2H, PCH_2), 1.03 (d, 6H, $^2J_{H,P}$ 7 Hz, PCH_3), 1.02 (m, 2H, PCH_2), 0.98 (d, 6H, $^2J_{H,P}$ 6 Hz, PCH_3), 0.91 (m, 2H, PCH_2), 0.91 (d, 6H, $^2J_{H,P}$ 3 Hz, PCH_3), –14.55 (p, 1H, $^2J_{H,P}$ 20 Hz, Mn*H*). ^{13}C{^{1}H} NMR (C_6D_6, 151 MHz, 300 K): δ 147.34 (s, *i*), 137.03 (s, *o*), 127.37 (s, *m*), 127.23 (s, *p*), 32.76 (m, PCH_2), 32.15 (m, PCH_2), 23.66 (d, $^1J_{C,P}$ 6 Hz, PCH_3), 23.62 (d, $^1J_{C,P}$ 6 Hz, PCH_3), 22.65 (d, $^1J_{C,P}$ 15 Hz, PCH_3), 22.55 (d, $^1J_{C,P}$ 16 Hz, PCH_3), 21.81 (d, $^1J_{C,P}$ 17 Hz, PCH_3), 17.25 (d, $^1J_{C,P}$ 25 Hz, PCH_3). ^{29}Si{^{1}H} NMR (C_6D_6, 119 MHz, 300 K): δ –4.20 (m). ^{29}Si NMR (d^8 toluene, 119 MHz, 300 K): δ –4.18 (t of m, $^1J_{Si,H}$ 168 Hz). ^{31}P{^{1}H} NMR (C_6D_6, 243 MHz, 300 K): δ 67.42 (s, 2P), 60.24 (s, 2P). Anal. Found (Calcd): C, 50.47 (50.52); H, 8.49 (8.30).

[(dmpe)$_2$MnH($SiH_2{}^nBu)_2$] (4b). An excess of *n*-butyl silane (293 mg, 3.32 mmol) was added to a solution of [(dmpe)$_2$MnH(C_2H_4)] (**1**) (503.2 mg, 1.31 mmol) in 25 mL of benzene. The reaction mixture was stirred in a 50 mL sealed flask at 60 °C for 2 days, after which time the solvent was removed *in vacuo* leading to a yellow solid. Note that ethane is formed as a by-product in this reaction so after a few hours the reaction mixture was temporarily allowed to cool to room temperature and the excess gas was vented into the Schlenk line before continuing at 60 °C. Recrystallization in hexanes at –30 °C yielded 357.6 mg of **4b**, and removing the solvent *in vacuo* from the mother liquor and recrystallization of the residue in toluene at –30 °C yielded an additional 178.5 mg, for a total yield of 77% (536.1 mg, 1.01 mmol) of yellow powder. ^{1}H NMR (C_6D_6, 600 MHz, 300 K): δ 4.53 (m with ^{29}Si sat., 2H, $^1J_{H,Si}$ 178 Hz, Si*H*), 4.36 (m with ^{29}Si sat., 2H, $^1J_{H,Si}$ 159 Hz, Si*H*), 1.95 (m, 4H, $SiH_2CH_2CH_2CH_2CH_3$), 1.67 (t of q, 4H, $^3J_{H,H}$ 7 Hz, $SiH_2CH_2CH_2CH_2CH_3$), 1.47 (m, 2H, PCH_2), 1.40 (d, 6H, $^2J_{H,P}$ 6 Hz, PCH_3), 1.31 (d, 6H, $^2J_{H,P}$ 6 Hz, PCH_3), 1.22 (m, 4H, $SiH_2CH_2CH_2CH_2CH_3$), 1.21 (m, 4H, PCH_2), 1.08 (t, 6H, $^3J_{H,H}$ 7 Hz, $SiH_2CH_2CH_2CH_2CH_3$), 1.03 (d, 6H, $^2J_{H,P}$ 6 Hz, PCH_3), 0.97 (d, 6H, $^2J_{H,P}$ 4 Hz, PCH_3), 0.84 (m, 2H, PCH_2), –13.27 (t, 1H, $^2J_{H,P}$ 17 Hz, Mn*H*). ^{13}C{^{1}H} NMR (C_6D_6, 151 MHz, 300 K): δ 34.72 (s, $SiH_2CH_2CH_2CH_2CH_3$), 33.94 (m, PCH_2), 30.12 (m, PCH_2), 27.12 (s, $SiH_2CH_2CH_2CH_2CH_3$), 24.00 (d, $^1J_{C,P}$ 6 Hz, PCH_3), 23.96 (d, $^1J_{C,P}$ 6 Hz, PCH_3), 21.60 (s, $SiH_2CH_2CH_2CH_2CH_3$), 20.55 (d, $^1J_{C,P}$ 13 Hz, PCH_3), 19.31 (d, $^1J_{C,P}$ 23 Hz, PCH_3), 17.97 (d, $^1J_{C,P}$ 15 Hz, PCH_3), 17.86 (d, $^1J_{C,P}$ 16 Hz, PCH_3), 14.53 (s, $SiH_2CH_2CH_2CH_2CH_3$). ^{29}Si{^{1}H} NMR (C_6D_6, 119 MHz, 300 K): δ 1.62 (p, $^2J_{Si,P}$ 23 Hz). ^{29}Si NMR (C_6D_6, 119 MHz, 300 K): δ 1.63 (t of m, $^1J_{Si,H}$ 165 Hz). ^{31}P{^{1}H} (C_6D_6, 243 MHz, 300 K): δ 72.62 (s, 2P), 58.56 (s, 2P). Anal. Found (Calcd): C, 45.17 (45.27); H, 10.39 (10.45).

[(dmpe)$_2$MnH(H_2)] (5). 98.7 mg (0.26 mmol) of [(dmpe)$_2$MnH(C_2H_4)] (**1**) was dissolved in 10 mL of benzene, and the resulting solution was placed in a sealed flask and freeze-pump-thawed (×3). The flask was placed under an atmosphere of hydrogen gas at –95 °C using a liquid nitrogen-acetone bath, sealed at this temperature, and warmed to room temperature to provide approx. 2 atm of hydrogen gas for reactivity. After stirring at 60 °C for 5 days, the solvent was removed *in vacuo* and the resulting solid was extracted with pentane. Removal of the pentane *in vacuo* yielded a crude pale yellow powder with >95% purity by NMR (77% isolated yield; 70.4 mg, 0.20 mmol). Recrystallization from a concentrated solution in pentane at –30 °C yielded 48.7 mg of pure **5** (0.14 mmol, 52%). NMR data matches that previously reported (with ^{31}P δ = 82 ppm).[2,41] X-ray quality crystals were obtained from a concentrated solution of **5** in hexanes at –30 °C.

[(dmpe)$_2$MnEt(CN^{t}Bu)] (6a). An excess of *tert*-butyl isonitrile (250 mg, 3.01 mmol) was added to a solution of [(dmpe)$_2$MnH(C_2H_4)] (**1**) (129.8 mg, 0.34 mmol) in 10 mL of benzene. The reaction mixture was stirred in a sealed flask at 80 °C for 5 h, after which the solvent was removed *in vacuo* leading to an orange oily solid. Recrystallization from hexamethyldisiloxane at –30 °C afforded 53.2 mg of yellow solid. Concentrating the mother liquor and allowing the solution to sit again at –30 °C afforded another 20.0 mg of the yellow solid, providing a combined yield of 46% (73.2 mg, 0.16 mmol). Upon dissolution in solution, the bulk of the sample was observed to be the *trans* isomer, but a small amount of *cis* isomer was observed in the baseline. To obtain NMR characterization of the *cis* isomer, the reaction was carried out on a smaller scale (13.5 mg **1** and 24 mg CN^{t}Bu) in approx. 1 mL of C_6D_6 at 50 °C for 1.5 h, which provided a 3 : 6 : 1 ratio of **1** : ***cis*-6a** : ***trans*-6a**, and was analyzed in situ (with excess free isonitrile present). This ratio could be improved to 6 : 12 : 1 by removing the solvent *in vacuo* and redissolving. X-ray quality crystals of ***trans*-6a** were obtained from a saturated solution in pentane at –30 °C. ***cis*-6a** (selected): ^{1}H NMR

(C_6D_6, 600 MHz, 300 K): δ 1.83 (t, 3H, $^3J_{H,H}$ 8 Hz, CH_2CH_3), 1.54 (d, 3H, $^2J_{H,P}$ 7 Hz, PCH_3), 1.47 (d, 3H, $^2J_{H,P}$ 6 Hz, PCH_3), 1.29 (m, 6H, PCH_3), 1.28 (s, 9H, $CNC(CH_3)_3$), 1.14 (d, 3H, $^2J_{H,P}$ 5 Hz, PCH_3), 1.04 (d, 3H, $^2J_{H,P}$ 3 Hz, PCH_3), 0.22 (m, 1H, CH_2CH_3), –0.12 (m, 1H, CH_2CH_3). $^{13}C\{^1H\}$ NMR (C_6D_6, 151 MHz, 300 K): δ 35.24 (m, PCH_2), 32.29 (s, $CNC(CH_3)_3$), 24.25 (s, PCH_3), 23.53 (d, $^3J_{C,P}$ 10 Hz, CH_2CH_3), 23.32 (d, $^1J_{C,P}$ 17 Hz, PCH_3), 22.22 (d, $^1J_{C,P}$ 16 Hz, PCH_3), 19.51 (s, PCH_3), 17.25 (d, $^1J_{C,P}$ 15 Hz, PCH_3), 14.25 (d, $^1J_{C,P}$ 13 Hz, PCH_3), –2.47 (m, CH_2CH_3). $^{31}P\{^1H\}$ NMR (C_6D_6, 243 MHz, 300 K): δ 81 (br. s, 1P), 74.43 (br. s, 1P), 61.58 (br. s, 2P). ^1H NMR (d^8-toluene 500 MHz, 207 K): δ 1.98 (t, 3H, $^3J_{H,H}$ 7 Hz, CH_2CH_3), 1.60 (d, 3H, $^2J_{H,P}$ 6 Hz, PCH_3), 1.51 (d, 3H, $^2J_{H,P}$ 6 Hz, PCH_3), 1.30 (m, 3H, PCH_3), 1.27 (s, 9H, $CNC(CH_3)_3$), 1.26 (m, 3H, PCH_3), 1.08 (d, 3H, $^2J_{H,P}$ 4 Hz, PCH_3), 1.01 (d, 3H, $^2J_{H,P}$ 3 Hz, PCH_3), 0.92 (d, 3H, $^2J_{H,P}$ 5 Hz, PCH_3), 0.88 (d, 3H, $^2J_{H,P}$ 3 Hz, PCH_3), 0.26 (m, 1H, CH_2CH_3),[74] –0.11 (m, 1H, CH_2CH_3).[74] $^{13}C\{^1H\}$ NMR (d^8-toluene, 126 MHz, 207 K): δ 53.98 (s, $CNC(CH_3)_3$), 34.88 (m, PCH_2), 33.00 (m, PCH_2), 32.01 (s, $CNC(CH_3)_3$), 30.88 (m, PCH_2), 29.57 (m, PCH_2), 23.82 (d, $^3J_{C,P}$ 11 Hz, CH_2CH_3), 23.51 (br. s, PCH_3), 22.94 (d, $^1J_{C,P}$ 17 Hz, PCH_3), 22.05 (d, $^1J_{C,P}$ 12 Hz, PCH_3), 21.50 (d, $^1J_{C,P}$ 15 Hz, PCH_3), 18.97 (s, PCH_3), 16.28 (d, $^1J_{C,P}$ 14 Hz, PCH_3), 13.94 (d, $^1J_{C,P}$ 12 Hz, PCH_3), 12.45 (m, PCH_3), –2.66 (m, CH_2CH_3). $^{31}P\{^1H\}$ (d^8-toluene, 202 MHz, 207 K): δ 82.02 (s, 1P), 75.24 (s, 1P), 62.09 (s, 1P), 61.63 (s, 1P). ***trans*-6a**: ^1H NMR (C_6D_6, 600 MHz, 300 K): δ 1.51 (m, 4H, PCH_2), 1.43 (m, 4H, PCH_2), 1.41 (t, 3H, $^3J_{H,H}$ 8 Hz,[75] CH_2CH_3), 1.40 (s, 12H, PCH_3), 1.29 (s, 12H, PCH_3), 1.12 (s, 9H, $CNC(CH_3)_3$), –0.47 (p of q, 2H, $^3J_{H,P}$ 8 Hz, $^3J_{H,H}$ 8 Hz, CH_2CH_3). $^{13}C\{^1H\}$ NMR (C_6D_6, 151 MHz, 300 K): δ 205.95 (s, $CNC(CH_3)_3$), 53.79 (s, $CNC(CH_3)_3$), 32.62 (s, $CNC(CH_3)_3$), 32.12 (app. p, PCH_2), 24.63 (s, CH_2CH_3), 21.03 (s, PCH_3), 16.49 (s, PCH_3), 1.40 (p, $^2J_{C,P}$ 17 Hz, CH_2CH_3). $^{31}P\{^1H\}$ (C_6D_6, 202 MHz, 300 K): δ 74.66 (s). ν(CN) (nujol) = ***cis*-6a**: 1915 cm^{-1}, ***trans*-6a**: 1828 cm^{-1}. ν(CN) (octane) = ***cis*-6a**: 1923 cm^{-1}, ***trans*-6a**: 1829 cm^{-1}. Found (Calcd): C, 49.25 (48.82); H, 9.60 (9.92); N, 2.79 (3.00).

[(dmpe)$_2$MnEt(CNXyl)] (6b). 143.1 mg (0.37 mmol) of [(dmpe)$_2$MnH(C_2H_4)] (**1**) and 292.7 mg (2.23 mmol) of *o*-xylyl isonitrile were dissolved in 10 mL of benzene. The reaction mixture was heated at 50-55 °C for 2 days, after which time the solvent was removed *in vacuo* to afford a dark brown oil. Attempts to recrystallize **6b** from a variety of solvents failed to yield a pure product. However, X-ray quality crystals were obtained by recrystallization from toluene layered with hexanes at –30 °C which resulted in a green-brown oily residue with a small number of small bright orange crystals which could be picked out manually. To obtain NMR characterization of the *trans* isomer, the mother liquor from the aforementioned crystallization was maintained at –40 °C, yielding a green solid which contained ***trans*-6b** and **7** in a 1 : 6 ratio. To obtain NMR characterization of the *cis* isomer, the reaction was carried out on a smaller scale (17.7 mg **1** and 23.2 mg CNXyl) in C_6D_6 at 50 °C for 2.5 h, which provided a 7 : 1.25 : 1 : 2.5 ratio of **1** : ***cis*-6b** : ***trans*-6b : 7**, and was analyzed in situ (with excess free isonitrile present). ***cis*-6b** (selected): ^1H NMR (C_6D_6, 600 MHz, 300 K): δ 6.95 (d, 2H, $^3J_{H,H}$ 7 Hz, *m*), 6.76 (m, 1H, *p*), 2.52 (s, 6H, xylyl-CH_3), 1.92 (t, 3H, $^3J_{H,H}$ 8 Hz, CH_2CH_3), 1.62 (m, 3H, PCH_3), 1.50 (d, 3H, $^2J_{H,P}$ 6 Hz, PCH_3), 1.30 (m, 3H, PCH_3), 0.27 (m, 1H, CH_2CH_3), 0.03 (m, 1H, CH_2CH_3). $^{13}C\{^1H\}$ NMR (C_6D_6, 151 MHz, 300 K): δ 23.8 (CH_2CH_3),[76] 21.11 (s, xylyl-CH_3), –1.3 (CH_2CH_3)[76]. ***trans*-6b**: ^1H NMR (C_6D_6, 600 MHz, 300 K): δ 6.93 (d, 2H, $^3J_{H,H}$ 7 Hz, *m*), 6.71 (t, 1H, $^3J_{H,H}$ 8 Hz, *p*), 2.33 (s, 6H, xylyl-CH_3), 1.54 (m, 8H, PCH_2), 1.37 (t, 3H, $^3J_{H,H}$ 8 Hz,[75] CH_2CH_3), 1.35 (s, 12H, PCH_3), 1.20 (m, 12H, PCH_3), –0.43 (p of q, 2H, $^3J_{H,P}$ 8 Hz, $^3J_{H,H}$ 8 Hz, CH_2CH_3). $^{13}C\{^1H\}$ NMR (C_6D_6, 151 MHz, 300 K): δ 136.28 (*i*),[76] 131.42 (s, *o*), 128.25 (m, *m*), 120.39 (s, *p*), 32.16 (m, PCH_2), 24.24 (m, CH_2CH_3), 21.20 (s, PCH_3), 20.81 (s, xylyl-CH_3), 16.27 (s, PCH_3), 3.37 (CH_2CH_3)[76]. $^{31}P\{^1H\}$ (C_6D_6, 202 MHz, 300 K): δ 75.85 (s).

[(dmpe)Mn(CNXyl)$_3${C(=NXyl)CEt(=NXyl)}] (7). The mixture of ***trans*-6b** and **7** (see synthesis of **6b**) was then heated under vacuum at 140 °C for 2 hours. The resulting brown solid resisted further purification (approximately 90% pure by NMR spectroscopy). However, **7** was characterized by NMR spectroscopy and X-ray quality crystals were obtained by recrystallization of the crude mixture of ***trans*-6b** and **7** (see synthesis of **6b**) from a dilute solution in hexanes at –30 °C. ^1H NMR (C_6D_6, 600 MHz, 300 K): δ 7.04 (d, 2H, $^3J_{H,H}$ 8 Hz, *m*), 6.73–6.82 {m, *m* (8H) and *p* (5H)}, 2.85 (q, 2H, $^3J_{H,H}$ 8 Hz, CH_2CH_3), 2.47 (s, 12H, xylyl-CH_3), 2.44 (s, 12H, xylyl-CH_3), 1.99 (br. s, 6H, xylyl-CH_3), 1.64 (d, 6H, $^2J_{H,P}$ 8 Hz, PCH_3), 1.34 (m, 4H, PCH_2), 1.20 (d, 6H, $^2J_{H,P}$ 7 Hz, PCH_3), 0.69 (t, 3H, $^3J_{H,H}$ 8 Hz, CH_2CH_3). $^{13}C\{^1H\}$ NMR (C_6D_6, 151 MHz, 300 K): δ 179.44 (s, CCH_2CH_3), 156.33, 150.51, 134.13, 133.80, 133.34, 133.11, 132.31, 131.01 (8 × s, *o* and *i*), 128.06 (m, *m*), 127.93 (m, *m*), 125.47 (s, *p*), 123.57 (s, *p*), 121.62 (s, *p*), 120.20 (s, *p*), 31.38 (m, PCH_2), 30.76 (m, PCH_2), 26.68 (s, CH_2CH_3), 20.71 (s, xylyl-CH_3), 20.39 (s, xylyl-CH_3), 20.05 (s, xylyl-CH_3), 19.14 (s, xylyl-CH_3), 17.34 (d, $^1J_{C,P}$ 20 Hz, PCH_3), 16.82 (d, $^1J_{C,P}$ 20 Hz, PCH_3), 9.02 (s, CH_2CH_3). $^{31}P\{^1H\}$ (C_6D_6, 243 MHz, 300 K): δ 66.15 (s, 1P), 53.90 (s, 1P).

ASSOCIATED CONTENT

Supporting Information

The Supporting Information is available free of charge on the ACS Publications website at xxxxxxxxxxxxx. This data includes crystallographic details, computational results (tables of bonding parameters, bond orders, energies, Hirschfeld charges, geometry optimized coordinates, selected fragment calculations, selected ETS-NOCV calculations, figures of geometry optimized structures, and potential energy profiles), and selected ^1H, ^{13}C, ^{29}Si, and ^{31}P NMR spectra of complexes **4a-b**, **6a-b**, and **7** (PDF).

Accession Codes

CCDC 1846647−1846652 contain the supplementary crystallographic data for this paper. These data can be obtained free of charge via www.ccdc.cam.ac.uk/data_request/cif, by emailingdata_request@ccdc.cam.ac.uk, or by contacting The Cambridge Crystallographic Data Centre, 12 Union Road, Cambridge CB2 1EZ, UK; fax: +44 1223 336033.

AUTHOR INFORMATION

Corresponding Author

* D.J.H.E.: tel, 905-525-9140 x23307; fax, 905-522-2509; e-mail, emslied@mcmaster.ca

Notes

The authors declare no competing financial interests.

ACKNOWLEDGMENT

D.J.H.E. thanks Intel Corporation for funding of a portion of this work through the Semiconductor Research Corporation (SRC), and the NSERC of Canada for a Discovery Grant. We are grateful to Dr. Yurij Mozharivskyj and Fang Yuan for collection of X-ray diffraction data for **6b** and **7** while the department's diffractometer was out of commission, and for the assistance of Dr. Bob Berno and Rashik Ahmed in conducting NMR experiments. Also, we are grateful to Dr. Alex Adronov and Karen Neumann for the use of their IR spectrometers.

REFERENCES

1. Girolami, G. S.; Wilkinson, G.; Thornton-Pett, M.; Hursthouse, M. B. Hydrido, Alkyl, and Ethylene 1,2-Bis(dimethylphosphino)ethane Complexes of Manganese and the Crystal Structures of $MnBr_2$(dmpe)$_2$, [Mn(AlH_4)(dmpe)$_2$]$_2$ and $MnMe_2$(dmpe)$_2$, *J. Am. Chem. Soc.* **1983**, *105*, 6752-6753.

2. Girolami, G. S.; Howard, C. G.; Wilkinson, G.; Dawes, H. M.; Thornton-Pett, M.; Motevalli, M.; Hursthouse, M. B. Alkyl, Hydrido, and Tetrahydroaluminato Complexes of Manganese with 1,2-Bis(dimethylphosphino)ethane (dmpe). X-Ray Crystal Structures of $Mn_2(\mu\text{-}C_6H_{11})_2(C_6H_{11})_2(\mu$-dmpe), (dmpe)$_2$Mn(μ-H)$_2$AlH(μ-H)$_2$AlH(μ-$H_2$)Mn(dmpe)$_2$, and Li_4{MnH(C_2H_4)-

$[CH_2(Me)PCH_2CH_2PMe_2]_2\}_2 \cdot 2Et_2O$, *J. Chem. Soc., Dalton Trans.* **1985**, 921-929.

3. Price, J. S.; Emslie, D. J. H.; Britten, J. F. Manganese Silylene Hydride Complexes: Synthesis and Reactivity with Ethylene to Afford Silene Hydride Complexes, *Angew. Chem., Int. Ed.* **2017**, *56*, 6223-6227.

4. Waterman, R.; Hayes, P. G.; Tilley, T. D. Synthetic Development and Chemical Reactivity of Transition-Metal Silylene Complexes, *Acc. Chem. Res.* **2007**, *40*, 712-719.

5. Doherty, N. M.; Bercaw, J. E. Kinetics and Mechanism of the Insertion of Olefins into Transition-Metal-Hydride Bonds, *J. Am. Chem. Soc.* **1985**, *107*, 2670-2682.

6. Yasuda, H.; Yamamoto, H.; Arai, T.; Nakamura, A.; Chen, J.; Kai, Y.; Kasai, N. Facile Synthesis and Stereochemistry of Alkyne Complexes from Cp_2MH and $Cp_2MCH_2CH_2R$ (M = Nb, Ta), *Organometallics* **1991**, *10*, 4058-4066.

7. van Asselt, A.; Trimmer, M. S.; Henling, L. M.; Bercaw, J. E. Dioxygen-Derived Peroxo-Alkyl Complexes of Permethyltantalocene. Structural Characterization of $(\eta^5\text{-}C_5Me_5)_2Ta(\eta^2\text{-}O_2)(CH_2C_6H_5)$ and Acid-Catalyzed Rearrangement to Oxo-Alkoxide Derivatives, *J. Am. Chem. Soc.* **1988**, *110*, 8254-8255.

8. (a) Carmichael, A. J.; McCamley, A. Synthesis and Characterization of Cationic Bis(cyclopentadienyl)tungsten(IV) Complexes Containing Alkyl, Chloride and Hydride Ligands, *J. Chem. Soc., Dalton Trans.* **1995**, 3125-3129; (b) Chernega, A.; Cook, J.; Green, M. L. H.; Labella, L.; Simpson, S. J.; Souter, J.; Stephens, A. H. H. New *ansa*-2,2-bis(η-cyclopentadienyl)propane molybdenum and tungsten compounds and intramolecular hydrogen-deuterium exchange in methyl-hydride and ethyl-hydride derivatives, *J. Chem. Soc., Dalton Trans.* **1997**, 3225-3243.

9. Dudle, B.; Rajesh, K.; Blacque, O.; Berke, H. Rhenium in Homogeneous Catalysis: ReBrH(NO)(labile ligand)(large-bite-angle diphosphine) Complexes as Highly Active Catalysts in Olefin Hydrogenations, *J. Am. Chem. Soc.* **2011**, *133*, 8168-8178.

10. Bennett, M. A.; McMahon, I. J.; Pelling, S. The Protonation of Arene-Bis(ethylene) Complexes of Ruthenium and Osmium, *J. Organomet. Chem.* **1990**, *382*, 175-184.

11. (a) Brookhart, M.; Lincoln, D. M. Comparison of Migratory Aptitudes of Hydride and Alkyl Groups in β-Migratory Insertion Reactions of $Cp^*(P(OMe)_3)Rh(C_2H_4)R^+$ (R = H, CH_2CH_3), *J. Am. Chem. Soc.* **1988**, *110*, 8719-8720; (b) Bianchini, C.; Meli, A.; Peruzzini, M.; Vizza, F.; Frediani, P.; Ramirez, J. A. Tripodal Polyphosphine Ligands in Homogeneous Catalysis. 1. Hydrogenation and Hydroformylation of Alkynes and Alkenes assisted by Organorhodium Complexes with $Me(CH_2PPh_2)_3$, *Organometallics* **1990**, *9*, 226-240.

12. (a) Padilla-Martínez, I. I.; Poveda, M. L.; Carmona, E.; Monge, M. A.; Ruiz-Valero, C. Synthesis and Reactivity of $[Ir(C_2H_4)_2Tpm^{Me2}]PF_6$ (Tpm^{Me2} = Tris(3,5-dimethylpyrazolyl)-methane): Comparison with the Analogous Tp^{Me2} Derivatives (Tp^{Me2} = Hydrotris(3,5-dimethylpyrazolyl)borate), *Organometallics* **2002**, *21*, 93-104; (b) García-Camprubí, A.; Martín, M.; Sola, E. Addition of Water Across Si-Ir Bonds in Iridium Complexes with *κ-P,P,Si* (biPSi) Pincer Ligands, *Inorg. Chem.* **2010**, *49*, 10649-10657.

13. Shultz, L. H.; Tempel, D. J.; Brookhart, M. Palladium(II) β-Agostic Alkyl Cations and Alkyl Ethylene Complexes: Investigation of Polymer Chain Isomerization Mechanisms, *J. Am. Chem. Soc.* **2001**, *123*, 11539-11555.

14. Shiotsuki, M.; White, P. S.; Brookhart, M.; Templeton, J. L. Mechanistic Studies of Platinum(II)-Catalyzed Ethylene Dimerization: Determination of Barriers to Migratory Insertion in Diimine Pt(II) Hydrido Ethylene and Ethyl Ethylene Intermediates, *J. Am. Chem. Soc.* **2007**, *129*, 4058-4067.

15. Green, M. L. H.; Wong, L. L. Is a 16-Electron, σ-Ethyl Intermediate Necessary for Hydrogen Scrambling in Ethylene-Hydride Complexes?, *J. Chem. Soc., Chem. Commun.* **1988**, 677-679.

16. Faller, J. W.; Fontaine, P. P. Stereoselectivity in a Chiral Ruthenium Ethylene Hydride Complex: Evidence of an Agostic Intermediate, *Organometallics* **2007**, *26*, 1738-1743.

17. Findlater, M.; Cartwright-Sykes, A.; White, P. S.; Schauer, C. K.; Brookhart, M. Role of Coordination Geometry in Dictating the Barrier to Hydride Migration in d^6 Square-Pyramidal Iridium and Rhodium Pincer Complexes, *J. Am. Chem. Soc.* **2011**, *133*, 12274-12284.

18. (a) Tempel, D. J.; Brookhart, M. The Dynamics of the *β*-Agostic Isopropyl Complex $(ArN{=}C(R)\text{-}C(R){=}NAr)Pd(CH(CH_2\text{-}\mu\text{-}H)(CH_3))^+BAr'_4^-$ (Ar = 2,6-C_6H_3(*i*-Pr)$_2$): Evidence for In-Place Rotation versus Dissociation of the Agostic Methyl Group, *Organometallics* **1998**, *17*, 2290-2296; (b) McNally, J. P.; Cooper, N. J. Mechanism of the Conversion of Intermediate 16-Electron Tungstenocene Alkyls into Alkene Hydrides and Fluxionality within $[W(\eta\text{-}C_5H_5)_2(CH_2{=}CHCH_3)H][PF_6]$, *Organometallics* **1988**, *7*, 1704-1715; (c) Casey, C. P.; Yi, C. S. Acid-Catalyzed Isomerization and Deuterium Exchange of Rhenium Alkene Complexes Via In-Place Rotation of an Agostic Alkylrhenium Cation, *Organometallics* **1991**, *10*, 33-35; (d) Bercaw, J. E.; Burger, B. J.; Green, M. L. H.; Santarsiero, B. D.; Sella, A.; Trimmer, M. S.; Wong, L. L. A New Mechanism for Exchange Processes observed in the Compounds $[M(\eta\text{-}C_5H_5)_2(exo\text{-}\eta\text{-}RCH{=}CH_2)H]$, M = Nb and Ta, *J. Chem. Soc., Chem. Commun.* **1989**, 734-736.

19. (a) Green, M. L. H.; Wong, L.-L. η-Benzenebis-(trimethylphosphine)iron as a Precursor to $Fe(\eta\text{-}C_5R_5)(PMe_3)_2$ Derivatives, R = H,Me: the Equilibrium $[Fe](PMe_3)Et \rightleftharpoons [Fe](\eta\text{-}C_2H_4)H + PMe_3$, where [Fe] = $Fe(\eta\text{-}C_5Me_5)(PMe_3)$, *J. Chem. Soc., Chem. Commun.* **1984**, 1442-1443; (b) Green, M. L. H.; Wong, L.-L. η-Benzenebis(trimethylphosphine)iron as a Precursor to $[Fe(\eta\text{-}C_5R_5)(PMe_3)_2]$ (R = H or Me) Derivatives: the Equilibrium $[Fe](PMe_3)Et \rightleftharpoons [Fe](\eta\text{-}C_2H_4)H + PMe_3$, where [Fe] = $Fe(\eta\text{-}C_5Me_5)(PMe_3)$, *J. Chem. Soc., Dalton Trans.* **1987**, 411-416.

20. (a) Bianchini, C.; Meli, A.; Peruzzini, M.; Frediani, P.; Bohanna, C.; Esteruelas, M. A.; Oro, L. A. Selective Hydrogenation of 1-Alkynes to Alkenes Catalyzed by an Iron(II) *cis*-Hydride η^2-Dihydrogen Complex. A Case of Intramolecular Reaction between η^2-H_2 and *σ*-Vinyl Ligands, *Organometallics* **1992**, *11*, 138-145; (b) Hills, A.; Hughes, D. L.; Jimenez-Tenorio, M.; Leigh, G. J.; Rowley, A. T. Bis[1,2-bis(dimethylphosphino)ethane]dihydrogenhydrido-iron(II) Tetraphenylborate as a Model for the Function of Nitrogenases, *J. Chem. Soc., Dalton Trans.* **1993**, 3041-3049; (c) Gao, Y.; Holah, D. G.; Hughes, A. N.; Spivak, G. J.; Havighurst, M. D.; Magnuson, V. R. Some reaction chemistry of *trans*-$[Fe(H)(\eta^2\text{-}H_2)(\eta^2\text{-dppm})_2][BF_4]$. The crystal and molecular structure of *trans*-$[Fe(H)(CH_3CN)(\eta^2\text{-dppm})_2][BF_4]$, dppm = bis(diphenylphosphino)methane, *Polyhedron* **1998**, *17*, 3881-3888.

21. (a) Kempter, A.; Gemel, C.; Cadenbach, T.; Fischer, R. A. Nickel olefin complexes supported by Ga^I(DDP), *Organometallics* **2007**, *26*, 4257-4264; (b) Goddard, R.; Krüger, C.; Pörschke, K. R.; Wilke, G. Elektronendichte-Verteilungen in Metallorganischen Verbindungen. Wechselnde Struktur-Und Bindungsverhältnisse in Dimeren Metallorganischen Nickel-Hydriden Mit Ionenpaar-Beziehungen zu den Hauptgruppen-Metallen Natrium und Lithium, *J. Organomet. Chem.* **1986**, *308*, 85-103; (c) Pörschke, K. R.; Kleimann, W.; Wilke, G.; Claus, K. H.; Krüger, C. Synthesis and Structure of $[Na(tmeda)_2]^+[HNi_2(C_2H_4)_4]^-$, *Angew. Chem., Int. Ed. Engl.* **1983**, *22*, 991-992.

22. Klein, H. F.; Hammer, R.; Gross, J.; Schubert, U. Olefin-Insertion into Cobalt(d^8) Complexes - Structure of Ethylene(phenyl)tris(trimethylphosphane)cobalt, *Angew. Chem., Int. Ed. Engl.* **1980**, *19*, 809-810.

23. Wadepohl, H.; Kohl, U.; Bittner, M.; Köppel, H. Experimental and Theoretical Study of the Hydride Migration to Ethylene in an Electron-Rich Cobalt Complex, *Organometallics* **2005**, *24*, 2097-2105.

24. Thompson, M. E.; Baxter, S. M.; Bulls, A. R.; Burger, B. J.; Nolan, M. C.; Santarsiero, B. D.; Schaefer, W. P.; Bercaw, J. E. "σ-Bond Metathesis" for C-H Bonds of Hydrocarbons and Sc-R (R = H, alkyl, aryl) Bonds of Permethylscandocene Derivatives. Evidence for Noninvolvement of the π System in Electrophilic Activation of Aromatic and Vinylic C-H Bonds, *J. Am. Chem. Soc.* **1987**, *109*, 203-219.

25. (a) Luinstra, G. A.; ten Cate, L. C.; Heeres, H. J.; Pattiasina, J. W.; Meetsma, A.; Teuben, J. H. Synthesis and Reactivity of Tervalent Paramagnetic Titanium Compounds (η^5-$C_5Me_5)_2TiR$: Molecular Structure of (η^5-$C_5Me_5)_2TiCH_2CMe_3$, *Organometallics* **1991**, *10*, 3227-3237; (b) Dawoodi, Z.; Green, M. L. H.; Mtetwa, V. S. B.; Prout, K. Evidence for a Direct Bonding Interaction between Titanium and a β-C-H Moiety in a Titanium-Ethyl Compound; X-Ray Crystal-Structure of [$Ti(Me_2PCH_2CH_2PMe_2)EtCl_3$], *J. Chem. Soc., Chem. Commun.* **1982**, 802-803; (c) Haaland, A.; Scherer, W.; Ruud, K.; McGrady, G. S.; Downs, A. J.; Swang, O. On the Nature and Incidence of β-Agostic Interactions in Ethyl Derivatives of Early Transition Metals: Ethyltitanium Trichloride and Related Compounds, *J. Am. Chem. Soc.* **1998**, *120*, 3762-3772; (d) Lukens, W. W.; Smith III, M. R.; Andersen, R. A. A π-Donor Spectrochemical Series for X in ($Me_5C_5)_2TiX$, and β-Agostic Interactions in X=Et and N(Me)Ph, *J. Am. Chem. Soc.* **1996**, *118*, 1719-1728.

26. Scherer, W.; Priermeier, T.; Haaland, A.; Volden, H. V.; McGrady, G. S.; Downs, A. J.; Boese, R.; Bläser, D. Molecular Structures of $EtTiCl_3$ and $EtTiCl_3$(dmpe) (dmpe = $Me_2PCH_2CH_2PMe_2$): New Insights into β-Agostic Bonding, *Organometallics* **1998**, *17*, 4406-4412.

27. (a) Conroy-Lewis, F. M.; Mole, L.; Redhouse, A. D.; Litster, S. A.; Spencer, J. L. Synthesis of Coordinatively Unsaturated Diphosphine Nickel(II) and Palladium(II) β-Agostic Ethyl Cations: X-ray Crystal Structure of [$Ni(Bu^t_2P(CH_2)_2PBu^t_2)(C_2H_5)][BF_4]$, *J. Chem. Soc., Chem. Commun.* **1991**, 1601-1603; (b) Wiencko, H. L.; Kogut, E.; Warren, T. H. Neutral β-diketiminato nickel(II) monoalkyl complexes, *Inorg. Chim. Acta* **2003**, *345*, 199-208.

28. Kogut, E.; Zeller, A.; Warren, T. H.; Strassner, T. Structure and Dynamics of Neutral β-H Agostic Nickel Alkyls: A Combined Experimental and Theoretical Study, *J. Am. Chem. Soc.* **2004**, *126*, 11984-11994.

29. (a) Leatherman, M. D.; Svejda, S. A.; Johnson, L. K.; Brookhart, M. Mechanistic Studies of Nickel(II) Alkyl Agostic Cations and Alkyl Ethylene Complexes: Investigations of Chain Propagation and Isomerization in (α-diimine)Ni(II)-Catalyzed Ethylene Polymerization, *J. Am. Chem. Soc.* **2003**, *125*, 3068-3081; (b) Xu, H. W.; White, P. B.; Hu, C. H.; Diao, T. N. Structure and Isotope Effects of the β-H Agostic (α-Diimine)Nickel Cation as a Polymerization Intermediate, *Angew. Chem., Int. Ed.* **2017**, *56*, 1535-1538.

30. Brookhart, M.; Lincoln, D. M.; Volpe Jr., A. F.; Schmidt, G. F. Ligand and Substituent Effects on the Dynamics and Structure of Agostic Complexes of the Type $C_5R_5(L)Co(CH_2CHR'$-μ-$H)^+BF_4^-$ (L = $P(OMe)_3$, PMe_3; R = H, Me; R' = H, Me), *Organometallics* **1989**, *8*, 1212-1218.

31. Brookhart, M.; Lincoln, D. M.; Bennett, M. A.; Pelling, S. Dynamics of Agostic Complexes of the Type $[C_5R_5(C_2H_4)M(CH_2CH_2$-μ-$H)]^+$. Energy Differences between and Ancillary Ligand Control of Agostic and Terminal Hydride Structures, *J. Am. Chem. Soc.* **1990**, *112*, 2691-2694.

32. Lide, D., Structure of Free Molecules in the Gas Phase. In *CRC Handbook of Chemistry and Physics*, 98 ed.; Rumble, J. R., Ed. CRC Press 2018.

33. Jonas, K.; Häselhoff, C. C.; Goddard, R.; Krüger, C. Manganese(II) cyclopentadienide and (cyclopentadienyl)manganese-(biphenyl) as starting materials for the synthesis of carbonyl free organomanganese complexes, *Inorg. Chim. Acta* **1992**, *198-200*, 533-541.

34. The reaction of **1** with 10 equivalents of H_3SiPh proceeded faster than the analogous reaction with 5 equivalents, implying that isomerization of [$(dmpe)_2MnH(C_2H_4)$] to an ethyl isomer is not the rate determining step in this reaction.

35. Komuro, T.; Okawara, S.; Furuyama, K.; Tobita, H. Silane(silyl) and Bis(silyl)hydrido Manganese Complexes with Different Mn···H···Si Interaction: Observation of Gradual Si-H Bond Activation on the Metal Center, *Chem. Lett.* **2012**, *41*, 774-776.

36. Groom, C. R.; Bruno, I. J.; Lightfoot, M. P.; Ward, S. C. The Cambridge Structural Database, *Acta Cryst.* **2016**, *B72*, 171-179.

37. Lide, D., Characteristic Bond Lengths in Free Molecules. In *CRC Handbook of Chemistry and Physics*, 98 ed.; Rumble, J. R., Ed. CRC Press 2018.

38. Mantina, M.; Valero, R.; Cramer, C.; Truhlar, D., Atomic Radii of the Elements. In *CRC Handbook of Chemistry and Physics*, 98 ed.; Rumble, J. R., Ed. CRC Press 2018.

39. (a) Corey, J. Y.; Braddock-Wilking, J. Reactions of Hydrosilanes with Transition-Metal Complexes: Formation of Stable Transition-Metal Silyl Compounds, *Chem. Rev.* **1999**, *99*, 175-292; (b) Corey, J. Y. Reactions of Hydrosilanes with Transition Metal Complexes and Characterization of the Products, *Chem. Rev.* **2011**, *111*, 863-1071; (c) Corey, J. Y. Reactions of Hydrosilanes with Transition Metal Complexes, *Chem. Rev.* **2016**, *116*, 11291-11435.

40. Measured from ^1H–^{29}Si HMBC spectroscopy. Resolution limitations prevented measurement for **2b**.

41. (a) Meixner, P.; Batke, K.; Fischer, A.; Schmitz, D.; Eickerling, G.; Kalter, M.; Ruhland, K.; Eichele, K.; Barquera-Lozada, J. E.; Casati, N. P. M.; Montisci, F.; Macchi, P.; Scherer, W. J(Si,H) Coupling Constants of Activated Si-H Bonds, *J. Phys. Chem. A* **2017**, *121*, 7219-7235; (b) Nikonov, G. Recent Advances in Nonclassical Interligand Si□□□H Interactions, *Adv. Organomet. Chem.* **2005**, *53*, 217-309.

42. Perthuisot, C.; Fan, M.; Jones, W. D. Catalytic Thermal C-H Activation with Manganese Complexes: Evidence for η^2-H_2 Coordination in a Neutral Manganese Complex and Its Role in C-H Activation, *Organometallics* **1992**, *11*, 3622-3629.

43. An alternative reaction pathway involving initial dmpe cyclometallation and ethane elmination is unliketly, given that compound **1** is stable at the temperature of reaction, and ethane elmlination would almost certainly be irreversible.

44. (a) Braga, D.; Grepioni, F.; Biradha, K.; Desiraju, G. R. Agostic interactions in organometallic compounds. A Cambridge Structural Database study, *J. Chem. Soc., Dalton Trans.* **1996**, 3925-3930; (b) Brookhart, M.; Green, M. L. H.; Parkin, G. Agostic interactions in transition metal compounds, *Proc. Natl. Acad. Sci. U. S. A.* **2007**, *104*, 6908-6914.

45. Bittner, M.; Köppel, H. Quantum Dynamical Study of β-Hydrogen Transfer in Two Selected Late-Transition-Metal Complexes, *J. Phys. Chem. A* **2004**, *108*, 11116-11126.

46. An energy minimum with 2 unpaired electrons ($\mathbf{B^{trans}}$) was located for a 5-coordinate non-agostic isomer of **B** with a vacant coordination site *trans* to the ethyl ligand. This $\mathbf{B^{trans}}$ isomer is 85 kJ mol^{-1} higher in energy than $\mathbf{B^{\beta\text{-agostic}}}$. The restricted calculation (modelling a diamagnetic structure) afforded a minimum 5 kJ mol^{-1} higher in energy than the paramagnetic minimum, with a HOMO-LUMO gap of just 69 kJ mol^{-1} {cf. 250, 160, 115, and 116 kJ mol^{-1} for $\mathbf{B^{\beta\text{-agostic}}}$, $\mathbf{B^{\alpha\text{-agostic}}}$, $\mathbf{B^{109.5}}$, and $\mathbf{(BB)^{\ddagger}}$ respectively; none of these species geometry optimized to a lower energy paramgentic isomer}.

47. (a) Xu, R.; Bittner, M.; Klatt, G.; Köppel, H. Influence of Ligands on the Dynamics of Hydrogen Elimination in Cationic Complexes of Co and Rh, *J. Phys. Chem. A* **2008**, *112*, 13139-13148; (b) Xu, R.; Klatt, G.; Wadepohl, H.; Köppel, H. Hydrogen Scrambling in $[(C_5R_5)(L)M(H)(C_2H_4)]^+$ (M = Co, Rh). Relation of Experimental Kinetic Data to the Barriers of the Elementary Reaction Steps, *Inorg. Chem.* **2010**, *49*, 3289-3296.

48. Due to approximately 50:50 positional disorder in the isonitrile ligand, two possible sets of N–$C_{terminal}$, C–N–C, and Mn–C–N values exist. The first set of values is: C(3)–N(1) and C(3A)–N(1A) = 1.207(5) and 1.214(4) Å; C(3)–N(1)–C(4) and C(3A)–N(1A)–C(4A) = 148.3(5)° and 146.0(5)°; Mn–C(3)–N(1) and Mn–C(3A)–N(1A) = 168.2(6)° and 171.0(6)°. The second set of values is: C(3)–N(1A) and C(3A)–N(1) = 1.307(5) and 1.362(5) Å; C(3A)–N(1)–C(4) and C(3)–N(1A)–C(4A) =137.4(4)° and 131.4(4)°; Mn–C(3)–N(1A) and Mn–C(3A)–N(1): 146.9(5)° and 144.7(6)°. Only the first set of values is consistent with literature values, and DFT calculations also afforded bond lengths and angles in much closer agreement to the first set of values: N–$C_{terminal}$ = 1.22 Å, C–N–C = 147.2°, and Mn–C–N = 169.2°. Therefore, only the first set of values is included in the caption to Figure 8 and discussed further in this manuscript.

49. Morris, R. J.; Girolami, G. S. Thirteen-Electron Manganese(II) Tetraalkyls. Synthesis, Characterization, and X-ray

Crystal Structures of $[Li(tmed)]_2[MnMe_4]$ and the "β-Unstable" Species $[Li(tmed)]_2[MnEt_4]$ and $[Li(tmed)]_2[Mn(CH_2CH_2\text{-}t\text{-}Bu)_4]$, *Organometallics* **1989**, *8*, 1478-1485.

50. (a) Treichel, P. M. Transition Metal-Isocyanide Complexes, *Adv. Organomet. Chem.* **1973**, *11*, 21-86; (b) Singleton, E.; Oosthuizen, H. E. Metal isocyanide complexes, *Adv. Organomet. Chem.* **1983**, *22*, 209-310.

51. Examples of manganese complexes with iminoacyl ligands (all of which are κ^2-coordinated) can be found in: (a) Motz, P. L.; Alexander, J. J.; Ho, D. M. Isocyanide Insertion Reactions of Manganese(I) Alkyl and Iminoacyl Complexes, *Organometallics* **1989**, *8*, 2589-2601; (b) Motz, P. L.; Williams, J. P.; Alexander, J. J.; Ho, D. M.; Ricci, J. S.; Miller Jr., W. T. Coupling of Iminoacyl Groups to Diazabutadienes on Manganese Carbonyl Complexes, *Organometallics* **1989**, *8*, 1523-1533; (c) Utz, T. L.; Leach, P. A.; Geib, S. J.; Cooper, N. J. Formation of the 1,4-Diazabutadien-2-yl Complex $[Mn(CNPh^*)_4\{C(=NPh^*)C(CH_3)=N(Ph^*)\}]$ through Methylation of a Manganese(–I) Isonitrilate, *Organometallics* **1997**, *16*, 4109-4114; (d) Becker, T. M.; Alexander, J. J.; Bauer, J. A. K.; Nauss, J. L.; Wireko, F. C. CNR and CO Insertion Reactions of 2,6-Xylyl Isocyanide with *p*-Chlorobenzylpentacarbonylmanganese, *Organometallics* **1999**, *18*, 5594-5605.

52. B. J. Burger, J. E. B., Vacuum Line Techniques for Handling Air-Sensitive Organometallic Compounds. In *Experimental Organometallic Chemistry - A Practicum in Synthesis and Characterization*, American Chemical Society: Washington, D.C., 1987; Vol. 357, pp 79-98.

53. Scherer, W.; Meixner, P.; Batke, K.; Barquera-Lozada, J. E.; Ruhland, K.; Fischer, A.; Eickerling, G.; Eichele, K. $J(Si,H)$ Coupling Constants in Nonclassical Transition-Metal Silane Complexes, *Angew. Chem., Int. Ed.* **2016**, *55*, 11673-11677.

54. (a) ADF2010, SCM, Theoretical Chemistry, Vrije Universiteit, Amsterdam, The Netherlands, http://www.scm.com; (b) Guerra, C. F.; Snijders, J. G.; te Velde, G.; Baerends, E. J. Towards an order-*N* DFT method, *Theor. Chem. Acc.* **1998**, *99*, 391-403; (c) te Velde, G.; Bickelhaupt, F. M.; Baerends, E. J.; Fonseca Guerra, C.; Van Gisbergen, S. J. A.; Snijders, J. G.; Ziegler, T. Chemistry with ADF, *J. Comput. Chem.* **2001**, *22*, 931-967.

55. Perdew, J. P.; Burke, K.; Ernzerhof, M. Generalized Gradient Approximation Made Simple, *Phys. Rev. Lett.* **1996**, *77*, 3865-3868.

56. (a) van Lenthe, E.; Baerends, E. J.; Snijders, J. G. Relativistic regular two-component Hamiltonians, *J. Chem. Phys.* **1993**, *99*, 4597-4610; (b) van Lenthe, E.; Baerends, E. J.; Snijders, J. G. Relativistic total energy using regular approximations, *J. Chem. Phys.* **1994**, *101*, 9783-9792; (c) van Lenthe, E.; Snijders, J. G.; Baerends, E. J. The zero-order regular approximation for relativistic effects: The effect of spin-orbit coupling in closed shell molecules, *J. Chem. Phys.* **1996**, *105*, 6505-6516; (d) van Lenthe, E.; van Leeuwen, R.; Baerends, E. J.; Snijders, J. G. Relativistic Regular Two-Component Hamiltonians, *Int. J. Quantum Chem.* **1996**, *57*, 281-293; (e) van Lenthe, E.; Ehlers, A.; Baerends, E. J. Geometry optimizations in the zero order regular approximation for relativistic effects, *J. Chem. Phys.* **1999**, *110*, 8943-8953.

57. (a) Grimme, S.; Antony, J.; Ehrlich, S.; Krieg, H. A consistent and accurate ab initio parametrization of density functional dispersion correction (DFT-D) for the 94 elements H-Pu, *J. Chem. Phys.* **2010**, *132*, 154104; (b) Grimme, S.; Ehrlich, S.; Goerigk, L. Effect of the Damping Function in Dispersion Corrected Density Functional Theory, *J. Comput. Chem.* **2011**, *32*, 1456-1465.

58. (a) Becke, A. D. A multicenter numerical integration scheme for polyatomic molecules, *J. Chem. Phys.* **1988**, *88*, 2547-2553; (b) Franchini, M.; Philipsen, P. H. T.; Visscher, L. The Becke Fuzzy Cells Integration Scheme in the Amsterdam Density Functional Program Suite, *J. Comput. Chem.* **2013**, *34*, 1819-1827.

59. (a) note 29 in Bulo, R.; Ehlers, A.; Grimme, S.; Lammertsma, K. Vinylphosphirane-Phospholene Rearrangements: Pericyclic [1,3]-Sigmatropic Shifts or Not? *J. Am. Chem. Soc.* **2002**, *124*, 13903-13910; (b) Pauncz, R. *Spin Eigenfunctions*; Plenum Press: New York, 1979; (c) Szabo, A.; Ostlund, N. *Modern Quantum Chemistry*; 1st ed. revised ed.; McGraw-Hill: New York, 1989.

60. (a) Mayer, I. Charge, Bond Order and Valence in the Ab Initio SCF Theory, *Chem. Phys. Lett.* **1983**, *97*, 270-274; (b) Mayer, I. Charge, Bond Order and Valence in the Ab Initio SCF Theory (Addendum), *Chem. Phys. Lett.* **1985**, *117*, 396; (c) Mayer, I. On Bond Orders and Valences in the *Ab Initio* Quantum Chemical Theory, *Int. J. Quantum Chem.* **1986**, *29*, 73-84; (d) Sannigrahi, A. B.; Kar, T. Three-center bond index, *Chem. Phys. Lett.* **1990**, *173*, 569-572; (e) Bridgeman, A. J.; Cavigliasso, G.; Ireland, L. R.; Rothery, J. The Mayer bond order as a tool in inorganic chemistry, *J. Chem. Soc., Dalton Trans.* **2001**, 2095-2108.

61. Gopinathan, M. S.; Jug, K. Valency. I. A Quantum Chemical Definition and Properties, *Theor. Chim. Acta* **1983**, *63*, 497-509.

62. (a) Nalewajski, R. F.; Mrozek, J. Modified Valence Indices from the Two-Particle Density Matrix, *Int. J. Quantum Chem.* **1994**, *51*, 187-200; (b) Nalewajski, R. F.; Mrozek, J.; Mazur, G. Quantum chemical valence indexes from the one-determinantal difference approach, *Can. J. Chem.* **1996**, *74*, 1121-1130; (c) Mrozek, J.; Nalewajski, R. F.; Michalak, A. Exploring Bonding Patterns of Molecular Systems using Quantum Mechanical Bond Multiplicities, *Pol. J. Chem.* **1998**, *72*, 1779-1791.

63. (a) Nalewajski, R. F.; Mrozek, J.; Michalak, A. Two-electron valence indices from the Kohn-Sham orbitals, *Int. J. Quantum Chem.* **1997**, *61*, 589-601; (b) Michalak, A.; DeKock, R. L.; Ziegler, T. Bond Multiplicity in Transition-Metal Complexes: Applications of Two-Electron Valence Indices, *J. Phys. Chem. A* **2008**, *112*, 7256-7263.

64. (a) Ziegler, T.; Rauk, A. CO, CS, N_2, PF_3, and $CNCH_3$ as σ Donors and π Acceptors. A Theoretical Study by the Hartree-Fock-Slater Transition-State Method, *Inorg. Chem.* **1979**, *18*, 1755-1759; (b) Ziegler, T.; Rauk, A. A Theoretical Study of the Ethylene-Metal Bond in Complexes between Cu^+, Ag^+, Au^+, Pt^0, or Pt^{2+} and Ethylene, Based on the Hartree-Fock-Slater Transition-State Method, *Inorg. Chem.* **1979**, *18*, 1558-1565; (c) Bickelhaupt, F. M.; Baerends, E. J., Kohn-Sham DFT: Predicting and Understanding Chemistry. In *Reviews in Computational Chemistry*, Boyd, D. B.; Lipkowitz, K. B., Eds. Wiley-VCH: New York, 2000; pp 1-86.

65. (a) Mitoraj, M. P.; Michalak, A.; Ziegler, T. A Combined Charge and Energy Decomposition Scheme for Bond Analysis, *J. Chem. Theory Comput.* **2009**, *5*, 962-975; (b) Mitoraj, M. P.; Michalak, A.; Ziegler, T. On the Nature of the Agostic Bond between Metal Centers and β-Hydrogen Atoms in Alkyl Complexes. An Analysis Based on the Extended Transition State Method and the Natural Orbitals for Chemical Valence Scheme (ETS-NOCV), *Organometallics* **2009**, *28*, 3727-3733.

66. (a) Bérces, A.; Dickson, R. M.; Fan, L.; Jacobsen, H.; Swerhone, D.; Ziegler, T. An implementation of the coupled perturbed Kohn-Sham equations: perturbation due to nuclear displacements, *Comput. Phys. Commun.* **1997**, *100*, 247-262; (b) Jacobsen, H.; Bérces, A.; Swerhone, D. P.; Ziegler, T. Analytic second derivatives of molecular energies: a density functional implementation, *Comput. Phys. Commun.* **1997**, *100*, 263-276; (c) Wolff, S. K. Analytical Second Derivatives in the Amsterdam Density Functional Package, *Int. J. Quantum Chem.* **2005**, *104*, 645-659.

67. The SCANFREQ command rescans a specific range of frequencies along a normal mode numerically as described in the ADF manual: https://www.scm.com/doc/ADF/Input/Frequencies.html#scanning-a-range-of-frequencies. References for numeric frequency calculations are as follows: (a) Fan, L.; Ziegler, T. Nonlocal Density Functional Theory as a Practical Tool in Calculations on Transition States and Activation Energies. Applications to Elementary Reaction Steps in Organic Chemistry, *J. Am. Chem. Soc.* **1992**, *114*, 10890-10897; (b) Fan, L.; Ziegler, T. Application of density-functional theory to infrared absorption intensity calculations on main group molecules, *J. Chem. Phys.* **1992**, *96*, 9005-9012.

68. (a) Autschbach, J.; Ziegler, T. Nuclear spin-spin coupling constants from regular approximate relativistic density functional calculations. I. Formalism and scalar relativistic results for heavy metal compounds, *J. Chem. Phys.* **2000**, *113*, 936-947; (b) Autschbach, J.; Ziegler, T. Nuclear spin-spin coupling constants from

regular approximate relativistic density functional calculations. II. Spin-orbit coupling effects and anisotropies., *J. Chem. Phys.* **2000**, *113*, 9410-9418.

69. (a) Grimme, S. Accurate Description of van der Waals Complexes by Density Functional Theory Including Empirical Corrections, *J. Comput. Chem.* **2004**, *25*, 1463-1473; (b) Ernzerhof, M.; Scuseria, G. E. Assessment of the Perdew-Burke-Ernzerhof exchange-correlation functional, *J. Chem. Phys.* **1999**, *110*, 5029-5036.

70. Spaltenstein, E.; Palma, P.; Kreutzer, K. A.; Willoughby, C. A.; Davis, W. M.; Buchwald, S. L. Preparation and X-ray Structure of $Cp_2Ti(Ph_2SiH_2)(PMe_3)$, *J. Am. Chem. Soc.* **1994**, *116*, 10308-10309.

71. Sheldrick, G. M. A short history of SHELX, *Acta Crystallogr., Sect. A: Found. Crystallogr.* **2008**, *64*, 112-122.

72. Sheldrick, G. M. Crystal structure refinement with SHELXL, *Acta Crystallogr., Sect. C: Struct. Chem.* **2015**, *71*, 3-8.

73. Dolomanov, O. V.; Bourhis, L. J.; Gildea, R. J.; Howard, J. A. K.; Puschmann, H. OLEX2: a complete structure solution, refinement and analysis program, *J. Appl. Crystallogr.* **2009**, *42*, 339-341.

74. ^{31}P decoupling collapsed the multiplet to a doublet ($^2J_{H,H}$ = 11 Hz) of quartets ($^3J_{H,H}$ = 7 Hz), measured at 500 MHz.

75. Coupling constant is derived from 1D TOCSY NMR spectroscopy conducted on a 500 MHz spectrometer.

76. Only observed through 2D NMR spectroscopy.

TOC Graphic: